



## Urban influence on the concentration and composition of submicron particulate matter in central Amazonia

Suzane S. de Sá (1), Brett B. Palm (2), Pedro Campuzano-Jost (2), Douglas A. Day (2), Weiwei Hu (2), Gabriel Isaacman-VanWertz<sup>a</sup> (3), Lindsay D. Yee (3), Joel Brito<sup>b</sup> (4), Samara Carbone<sup>c</sup> (4), Igor O. Ribeiro (5), Glauber G. Cirino<sup>d</sup> (6), Yingjun J. Liu<sup>e</sup> (1), Ryan Thalman<sup>f</sup> (7), Arthur Sedlacek (7), Aaron Funk (8), Courtney Schumacher (8), John E. Shilling (9), Johannes Schneider (10), Paulo Artaxo (4), Allen H. Goldstein (3), Rodrigo A.F. Souza (5), Jian Wang (7), Karena A. McKinney<sup>g</sup> (1), Henrique Barbosa (4), M. Lizabeth Alexander (11), Jose L. Jimenez (2), Scot T. Martin\* (1, 12)

- (1) School of Engineering and Applied Sciences, Harvard University, Cambridge, Massachusetts, USA  
(2) Department of Chemistry and Cooperative Institute for Research in Environmental Sciences, University of Colorado, Boulder, Colorado, USA  
(3) Department of Environmental Science, Policy, and Management, University of California, Berkeley, California, USA  
(4) Institute of Physics, University of São Paulo, São Paulo, Brazil  
(5) School of Technology, Amazonas State University, Manaus, Amazonas, Brazil  
(6) National Institute for Amazonian Research, Manaus, Amazonas, Brazil  
(7) Brookhaven National Laboratory, Upton, New York, USA  
(8) Department of Atmospheric Sciences, Texas A&M University, College Station, Texas, USA  
(9) Atmospheric Sciences and Global Change Division, Pacific Northwest National Laboratory, Richland, WA, USA  
(10) Particle Chemistry Department, Max Planck Institute for Chemistry, Mainz, Germany  
(11) Environmental Molecular Sciences Laboratory, Pacific Northwest National Laboratory, Richland, Washington, USA  
(12) Department of Earth and Planetary Sciences, Harvard University, Cambridge, Massachusetts, USA  
<sup>a</sup> Now at Department of Civil and Environmental Engineering, Virginia Tech, Blacksburg, Virginia, USA  
<sup>b</sup> Now at Laboratory for Meteorological Physics (LaMP), University Blaise Pascal, Aubière, France  
<sup>c</sup> Now at Federal University of Uberlândia, Uberlândia, Minas Gerais, Brazil  
<sup>d</sup> Now at Department of Meteorology, Geosciences Institute, Federal University of Pará, Belém, Brazil  
<sup>e</sup> Now at University of California, Berkeley, California, USA  
<sup>f</sup> Now at Department of Chemistry, Snow College, Richfield, Utah, USA  
<sup>g</sup> Now at Colby College, Waterville, Maine, USA

\*To Whom Correspondence Should be Addressed

*E-mail: [scot\\_martin@harvard.edu](mailto:scot_martin@harvard.edu)*

*<https://martin.seas.harvard.edu/>*



## 1 Abstract

2 Fundamental to quantifying the influence of human activities on climate and air quality is  
3 an understanding of how anthropogenic emissions affect the concentrations and composition of  
4 airborne particulate matter (PM). The central Amazon basin, especially around the city of  
5 Manaus, Brazil, has experienced rapid changes in the past decades due to ongoing urbanization.  
6 Herein, changes in the concentration and composition of submicron PM due to pollution  
7 downwind of the Manaus metropolitan region are reported as part of the GoAmazon2014/5  
8 experiment. A high-resolution time-of-flight aerosol mass spectrometer (HR-ToF-AMS) and a  
9 suite of other gas- and particle-phase instruments were deployed at the “T3” research site, 70 km  
10 downwind of Manaus, during the wet season. At this site, organic components represented on  
11 average  $79 \pm 7\%$  of the non-refractory  $PM_{10}$  mass concentration, which was in the same range as  
12 several upwind sites. The organic  $PM_{10}$  was, however, considerably more oxidized at T3  
13 compared to upwind measurements. Positive-matrix factorization (PMF) was applied to the time  
14 series of organic mass spectra collected at the T3 site, yielding three factors representing  
15 secondary processes ( $73 \pm 15\%$  of total organic mass concentration) and three factors  
16 representing primary anthropogenic emissions ( $27 \pm 15\%$ ). Fuzzy c-means clustering (FCM) was  
17 applied to the afternoon time series of concentrations of  $NO_y$ , ozone, total particle number, black  
18 carbon, and sulfate. Four clusters were identified and characterized by distinct airmass origins  
19 and particle compositions. Two clusters, Bkgd-1 and Bkgd-2, were associated with background  
20 conditions. Bkgd-1 appeared to represent near-field atmospheric PM production and oxidation of  
21 a day or less. Bkgd-2 appeared to represent material transported and oxidized for two or more  
22 days, often with out-of-basin contributions. Two other clusters, Pol-1 and Pol-2, represented the  
23 Manaus influence, one apparently associated with the northern region of Manaus and the other



24 with the southern region of the city. A composite of the PMF and FCM analyses provided  
25 insights into the anthropogenic effects on PM concentration and composition. The increase in  
26 mass concentration of submicron PM ranged from 25% to 200% under polluted compared to  
27 background conditions, including contributions from both primary and secondary PM.  
28 Furthermore, a comparison of PMF factor loadings for different clusters suggested a shift in the  
29 pathways of PM production under polluted conditions. Nitrogen oxides may have played a  
30 critical role in these shifts. Increased concentrations of nitrogen oxides can shift pathways of PM  
31 production from HO<sub>2</sub>-dominant to NO-dominant as well as increase the concentrations of  
32 oxidants in the atmosphere. Consequently, the oxidation of biogenic and anthropogenic precursor  
33 gases as well as the oxidative processing of pre-existing atmospheric PM can be accelerated. The  
34 combined set of results demonstrates the susceptibility of atmospheric chemistry, air quality, and  
35 associated climate forcing to anthropogenic perturbations over tropical forests.



## 1 **1. Introduction**

2           Secondary organic material (SOM) constitutes a large fraction of the atmospheric particle  
3 burden (Hallquist et al., 2009; Jimenez et al., 2009) and therefore has important effects on the  
4 Earth's radiation balance, atmospheric visibility, and human health. SOM is a complex mixture  
5 of compounds resulting from many chemical pathways, and the processes underlying the  
6 production of SOM remain poorly understood. Models are especially challenged to accurately  
7 represent production of SOM in regions where there is a mix of biogenic and anthropogenic  
8 emissions (de Gouw et al., 2008; Glasius and Goldstein, 2016; Shrivastava et al., 2017). Possible  
9 shifts in the contributing mechanisms of SOM production between background and polluted  
10 conditions must be understood and quantified for distinct environments on the globe to test and  
11 enable accurate modeling predictions.

12           Several field observations, mainly in mid-latitudes of the Northern Hemisphere, and  
13 modeling efforts have suggested that the production of SOM from biogenic precursor  
14 compounds becomes more efficient in polluted air (Weber et al., 2007; Goldstein et al., 2009;  
15 Hoyle et al., 2011; Huang et al., 2014; Zhang et al., in press). In the northeastern USA, de Gouw  
16 et al. (2005) showed that organic PM concentrations correlated well with anthropogenic tracers,  
17 yet the concentrations of anthropogenic precursors were insufficient to explain the observed PM.  
18 In the southeastern USA, observations suggested that organic PM was produced mainly from  
19 BVOCs, however modulated by anthropogenic emissions of NO<sub>x</sub> and SO<sub>2</sub> (Weber et al., 2007;  
20 Goldstein et al., 2009). In the western USA, ground and aircraft measurements observed the  
21 highest organic PM increases when air masses having high concentrations of biogenic VOCs  
22 (BVOCs) intercepted anthropogenic emissions (Setyan et al., 2012; Shilling et al., 2013). A  
23 metastudy for several locations in the USA concluded that downwind urban air had increased



24 organic PM concentrations due to the photochemical production of SOM (De Gouw and  
25 Jimenez, 2009). Models have estimated that 50 to 70% of the biogenic SOM mass concentration  
26 in several locations is modulated by anthropogenic emissions (Carlton et al., 2010; Heald et al.,  
27 2011; Spracklen et al., 2011). In addition, global-scale modeling studies have estimated an  
28 increase of 20% to 60% in the global annual mean SOM concentration relative to the pre-  
29 industrial period (Tsigaridis et al., 2006; Hoyle et al., 2009).

30 Many possible mechanisms may contribute to the effects of anthropogenic emissions on  
31 increased SOM production, including changes in gas-particle partitioning, new particle  
32 production and growth, and particle acidity. Changes in the concentrations of nitrogen oxides,  
33 however, should be regarded as a critical factor (Hoyle et al., 2011 and references therein).  
34 Different NO<sub>x</sub> regimes favor distinct gas-phase oxidation pathways, leading to different  
35 oxidation products and particle yields, as evidenced in isoprene photo-oxidation (Kroll et al.,  
36 2005, 2006; Hallquist et al., 2009; Worton et al., 2013; Liu et al., 2016b; Liu et al., 2016a). For  
37 tropical forests, isoprene emissions are especially important in PM production (Martin et al.,  
38 2010a; Chen et al., 2015). Under HO<sub>2</sub>-dominant conditions (i.e., low NO<sub>x</sub>), isoprene epoxydiols  
39 (IEPOX) are produced in the gas phase and, through heterogenous reactions involving sulfate,  
40 PM is produced (Paulot et al., 2009; Surratt et al., 2010). Depending on the relative importance  
41 of increased concentrations of sulfate and NO<sub>x</sub> associated with pollution in a given region, an  
42 enhancement or suppression of IEPOX-derived PM production relative to background conditions  
43 may occur (Xu et al., 2015a; de Sá et al., 2017).

44 Amazonia, the largest tropical forest in the world and a large global source of SOM, is  
45 comparatively understudied relative to northern mid-latitude regions, especially with respect to  
46 the influence of pollution on the SOM lifecycle (Martin et al., 2010a). Manaus, a city of over two



47 million people in the central Amazon, continuously releases an urban plume into an otherwise  
48 mostly unperturbed region (Kuhn et al., 2010; Martin et al., 2017). The region downwind of  
49 Manaus, especially in the wet season in the absence of regional fires (Artaxo et al., 2013), offers  
50 a natural laboratory for the investigation of biogenic-anthropogenic interactions and the resulting  
51 consequences for the amount and composition of PM in the region. As part of GoAmazon2014/5,  
52 de Sá et al. (2017) demonstrated that PM derived from IEPOX generally decreased under  
53 polluted compared to background conditions downwind of Manaus. Nitrogen oxides in the  
54 pollution plume suppressed the production of isoprene hydroxyhydroperoxides (Liu et al.,  
55 2016b), leading to a decrease in the production of gas phase IEPOX and consequently of IEPOX-  
56 derived PM (de Sá et al., 2017). IEPOX-derived PM was the exclusive focus of de Sá et al.  
57 (2017).

58         The present study investigates the influences of urban pollution on the concentration and  
59 composition of fine particles in central Amazonia, focusing on organic PM and its several  
60 component classes. The analysis employs data sets collected during the first Intensive Operating  
61 Period (IOP1) of the GoAmazon2014/5 experiment (Martin et al., 2016), corresponding to the  
62 wet season during the period of February 1 to March 31, 2014. A separate publication is planned  
63 for IOP2, corresponding to the dry season period of August 15 to October 15, when biomass  
64 burning emissions were prevalent (de Sá et al., in preparation). Herein, positive-matrix  
65 factorization (PMF) of organic mass spectra measured by aerosol mass spectrometry (AMS) in  
66 conjunction with a clustering analysis of pollution indicators by Fuzzy c-means are employed to  
67 investigate the changes in particle concentration and composition associated with the influence  
68 of urban pollution downwind of Manaus.



## 69 2. Methodology

### 70 2.1 Site description

71 The primary site of this study, named “T3” (3.2133 °S, 60.5987 °W), was located 70 km  
72 to the west of Manaus, Brazil, in central Amazonia (Martin et al., 2016). The site was situated in  
73 a pasture of 2.5 km × 2 km surrounded by forest. Auxiliary sites “T0a” and “T0t”, served as  
74 references for background conditions in relation to T3 (Figure S1). Site T0a (2.1466 °S,  
75 59.0050 °W) refers to the Amazonian Tall Tower Observatory (ATTO; Andreae et al., 2015),  
76 located 150 km to the northeast of Manaus. Site T0t (2.5946°S, 60.2093°W) was situated 60 km  
77 to the north-northwest of Manaus in the Cuieiras Biological Reserve (“ZF2”) and refers to tower  
78 “TT34”, established in 2008 for the AMAZE-08 experiment (Martin et al., 2010b). The T0 sites  
79 were typically upwind of Manaus, with only occasional transport of pollution to these sites  
80 (Andreae et al., 2015; Chen et al., 2015). Auxiliary site “T2” served as a reference for polluted  
81 conditions. This site was located just across the Rio Negro (3.1392°S, 60.1315°W), 8 km from  
82 the southwestern edge of Manaus and typically downwind of urban emissions during the  
83 daytime.

### 84 2.2 Aerosol Mass Spectrometry

85 Characterization of the atmospheric PM was obtained using a High-Resolution Time-of-  
86 Flight Aerosol Mass Spectrometer (hereafter AMS; Aerodyne, Inc., Billerica, Massachusetts,  
87 USA; DeCarlo et al., 2006; Canagaratna et al., 2007). Detailed aspects of the AMS operation in  
88 GoAmazon2014/5 were presented in de Sá et al. (2017). In brief, the instrument was housed  
89 within a temperature-controlled research container, and the inlet to the instrument sampled from  
90 5 m above ground level. Ambient measurements for this study were obtained every other 4 min.



91 The other 4 min were used for analysis of output from an oxidation flow reactor as presented in  
92 Palm et al. (2018).

93 Data analysis was performed using *SQUIRREL* (1.56D) and *PIKA* (1.14G) of the AMS  
94 software suite (Sueper and collaborators; DeCarlo et al., 2006). Organic, sulfate, ammonium,  
95 nitrate, and chloride PM mass concentrations were obtained from “V-mode” data. The choice of  
96 ions to fit was aided by “W-mode” data, which were collected for one of every five days.  
97 “Sulfate” and “nitrate” concentrations reported by the AMS may include contributions from both  
98 organic and inorganic species (Farmer et al., 2010; Liao et al., 2015). Organic and inorganic  
99 nitrate concentrations were estimated based on the ratio of  $\text{NO}_2^+$  to  $\text{NO}^+$  signal intensity, as  
100 described in Section S2 (Fry et al., 2009; Farmer et al., 2010; Fry et al., 2013). The organic  
101 elemental ratios, O:C and H:C, were calculated following the methods of Canagaratna et al.  
102 (2015).

### 103 **2.3 Auxiliary measurements and datasets**

104 In complement to the AMS data set, the analysis herein incorporated auxiliary gas and  
105 particle measurements from T3 (Martin et al., 2016). Mass concentrations of molecular and  
106 tracer organic species in the gas and particle phases were measured by a Semi-Volatile Thermal  
107 Desorption Aerosol Gas Chromatograph (SV-TAG) at a time resolution of one hour (Isaacman-  
108 VanWertz et al., 2016). Concentrations of volatile organic compounds (VOCs) were measured  
109 by a Proton-Transfer-Reaction Time-of-Flight Mass Spectrometer (PTR-ToF-MS; Liu et al.,  
110 2016b). In the Mobile Aerosol Observing System (MAOS) of the ARM Climate Research  
111 Facility (ACRF; Martin et al., 2016), measurements of  $\text{NO}_y$  were made using a  
112 chemiluminescence-based instrument (Air Quality Design). The raw  $\text{NO}_y$  measurements (10-s  
113 resolution) were averaged across 30-min intervals to dampen the influence of brief local events.



114 In addition, ozone concentrations were measured by an ultraviolet photometric analyzer (Thermo  
115 Fisher, model 49i, Ozone Analyzer). Particle number concentrations were measured by a  
116 Condensation Particle Counter (TSI, model 3772). Black carbon (BC) concentrations were  
117 measured both by a 7-wavelength aethalometer (Magee Scientific, model AE-31) and a Single  
118 Particle Soot Photometer (SP2; Droplet Measurement Techniques). The two datasets differed by  
119 a factor of up to three in absolute mass concentrations, as observed in other studies (Subramanian  
120 et al., 2007; Cappa et al., 2008; Lack et al., 2008), but they agreed well in the temporal trend.  
121 The analysis herein for BC is thus restricted to the temporal trends. Wind direction, solar  
122 irradiance, and precipitation rate were measured by the ARM Mobile Facility (AMF-1), which  
123 was also part of the ACRF.

124 Additional measurements from T0a, T0t, and T2 were also used in the analysis. At T2,  
125 non-refractory particle composition and concentration were measured by an Aerosol Chemical  
126 Speciation Monitor (ACSM; Brito et al., in preparation). ACSM measurements were also made  
127 at T0a during the wet season of 2015 (Carbone et al., in preparation). Further datasets collected  
128 by AMS at T0t during the wet season of 2008 (AMAZE-08 campaign) were used in the analysis  
129 (Chen et al., 2009; Schneider et al., 2011). AMS measurements made onboard the G-1 aircraft of  
130 the ARM Aerial Facility (AAF) during IOP1 also supported the analysis herein (Shilling et al., in  
131 preparation).

#### 132 **2.4 Air mass backtrajectories and precipitation rates**

133 Simulations of two-day backward air mass trajectories, starting at 100 m above T3, were  
134 made using HYSPLIT4 (Draxler and Hess, 1998). Input meteorological data were obtained  
135 from the Global Data Assimilation System (GDAS), provided by the NOAA Air Resources



136 Laboratory (ARL), on a regular grid of  $0.5^\circ \times 0.5^\circ$ , 18 pressure levels, and 3-h intervals.

137 Trajectory steps were calculated for every 12 min.

138 Information on precipitation along the trajectories was obtained from the S-band radar of  
139 the System for Amazon Protection (SIPAM) in Manaus (Machado et al., 2014). The radar had a  
140 beam width of  $1.8^\circ$ , and it scanned 17 elevation angles every 12 min. Data were recorded to a  
141 range of 240 km at 500-m gate spacing. The reflectivity fields were quality controlled to remove  
142 non-meteorological echo and calibrated against the satellite precipitation radar of the Tropical  
143 Rainfall Measuring Mission and Global Precipitation Measurement (TRMM-GPM; Kummerow  
144 et al., 1998; Hou et al., 2014). Ground clutter was used to analyze the stability of the calibration.  
145 The data were gridded at  $2 \text{ km} \times 2 \text{ km}$  in the horizontal and 0.5 km in the vertical using the  
146 NCAR *Radx* software. The reflectivity at 2.5 km in altitude was converted to rain rates based on  
147 the data sets of a Joss-Waldvogel disdrometer (Joss and Waldvogel, 1967), located at T3, 70 km  
148 downwind of the radar.

### 149 **3. Results and discussion**

#### 150 **3.1 Fine-mode PM composition**

151 The time series of mass concentrations of  $\text{PM}_{10}$  species at T3 during the wet season of  
152 2014 are plotted in Figure 1a. Organic material dominated the composition, contributing  $79 \pm 7\%$   
153 (average  $\pm$  one standard deviation), followed by sulfate ( $13 \pm 5\%$ ). The standard deviation  
154 quantifies the variability across the time series. Average non-refractory (NR)  $\text{PM}_{10}$  mass  
155 concentrations and compositions at T3 as well as at three other sites in the region are represented  
156 in Figure 1b. The two T0 sites corresponded to predominantly background conditions. By  
157 contrast, the T2 site represented conditions just downwind of Manaus, and depending on wind  
158 direction experienced fresh Manaus pollution or background air. The comparison in Figure 1b



159 demonstrates that the organic component consistently constituted 70% to 80% of NR-PM<sub>1</sub> across  
160 sites in this region in the wet season, for both background and polluted conditions, in line with  
161 previous observations (Chen et al., 2009; Martin et al., 2010a).

162 Even as the relative composition was similar across all sites, there were differences in the  
163 absolute mass concentrations (Figure 1b, top panel). The NR-PM<sub>1</sub> mass concentrations at the T0  
164 sites upwind of Manaus were approximately 1 µg m<sup>-3</sup>. The concentrations at the T2 site just  
165 downwind of Manaus were more than three times higher on average (3.3 µg m<sup>-3</sup>). Average  
166 concentrations at the T3 site (1.7 µg m<sup>-3</sup>), several hours downwind of Manaus, were lower  
167 compared to those at T2. This relative progression from T0, to T2, and then to T3 can be  
168 understood as a first-order quantification of the overall effect of Manaus emissions in increasing  
169 the airborne PM burden in the downwind region.

170 The diel trends of organic and sulfate mass concentrations across the four sites are shown  
171 in Figure 2. Lines represent means, solid markers show medians, and boxes span interquartile  
172 ranges. Organic mass concentrations and associated variability were higher at the T3 site  
173 compared to the T0 sites, markedly so in the afternoon hours. The greater variability at T3 is in  
174 line with a time-varying influence of Manaus emissions. This influence waxes and wanes with  
175 small northerly or southerly shifts of the trade winds as well as other changes in regional  
176 circulation tied to daily meteorology (Cirino et al., submitted). The higher afternoon mass  
177 concentrations at T3 can be attributed to a combination of (i) an oxidant-rich, sunlight-fed plume  
178 that increases the production rate of secondary PM and (ii) faster near-surface winds during the  
179 day that transport PM from Manaus to T3 with less loss by deposition and dispersion compared  
180 to more-stagnant air at night. Among all sites, the T2 observations had both the highest average  
181 organic mass concentrations and the largest variability. These characteristics of the T2 dataset



182 can be explained by a combination of (i) the proximity of the site to Manaus, (ii) the rapid and  
183 180° changes in wind direction caused by the intersection of the trade winds with a local river  
184 breeze (dos Santos et al., 2014), and (iii) possible contributions of emissions from brick kilns,  
185 located mostly southwest of the site, especially during night time (Martin et al., 2016; Cirino et  
186 al., submitted).

187 The diel trends of the sulfate mass concentrations were in large part similar to those of  
188 the organic mass concentrations. One distinction in the case of sulfate, however, is that the  
189 variability at the T0 sites is similar to that at the T3 site. The explanation is that the background  
190 sources of sulfate, including not only in-basin emissions but also out-of-basin long-range  
191 transport, are variable and significant enough to make the variability at the background sites  
192 similar to that at the T3 site (de Sá et al., 2017).

193 Overall, the organic PM<sub>1</sub> at T3 was highly oxidized, as indicated by the position of gray  
194 markers in the plot of Figure 3. By contrast, the blue markers represent the dataset collected at  
195 T2 during the same period. The datasets encompass all times of days and all conditions at both  
196 sites. Datasets from background sites collected in different years are shown in Figure S2. Points  
197 to the upper left represent more oxidized material, and points to the lower right represent less  
198 oxidized material (Ng et al., 2011a). The comparison depicted in Figure 3 illustrates the effects  
199 of the plume over the 4 h of transport from T2 to T3 (Cirino et al., submitted). The plot suggests  
200 that the enhanced oxidative cycle associated with higher OH and O<sub>3</sub> concentrations in the  
201 pollution plume might cause (i) the production of highly oxidized SOM, from both biogenic and  
202 anthropogenic precursors including aromatic compounds (Chhabra et al., 2011; Lambe et al.,  
203 2011), and (ii) the accelerated oxidative processing of pre-existing organic PM by OH and O<sub>3</sub>



204 (Martin et al., 2017). The implication is that the emissions from Manaus can significantly affect  
205 the mechanisms that produce or modify fine-mode PM over the tropical forest.

### 206 **3.2 Characterization of organic PM by positive-matrix factorization**

207 Positive-matrix factorization was applied to the time series of the organic component of  
208 the high-resolution “V mode” mass spectra (Ulbrich et al., 2009b). Diagnostics of the PMF  
209 analysis are presented in the Supplement (Section S1; Figures S3 and S4). Herein, “factor  
210 profile” and “factor loading” refer to the mathematical products of the multivariate statistical  
211 analysis, whereas “mass spectrum” and “mass concentration” refer to direct measurements.

212 A six-factor solution was obtained based both on the numerical diagnostics of the PMF  
213 algorithm and the judged scientific meaningfulness of the resolved factors (Section S1). The  
214 factor profiles, diel trends of the factor loadings, and the time series of the factor loadings and  
215 other related measurements are plotted in Figures 4a, 4b, and 4c, respectively. The inset of  
216 Figure 4a shows the mean fractional loading contribution of each factor during the analysis  
217 period. The correlations of factor loadings with co-located measurements of gas- and particle-  
218 phase species are shown in Figure 5.

219 The scientific interpretation of each factor was based on a combination of (i) the  
220 characteristics of the factor profile (i.e., “mass spectrum”), as referenced to a worldwide database  
221 of AMS spectra and PMF analyses (Ulbrich et al., 2009b; Ulbrich et al., 2009a, 2009c), and (ii)  
222 the temporal correlations between the factor loading and other co-located measurements. Three  
223 factors interpreted as primary emissions of organic PM were resolved: an anthropogenic-  
224 dominated factor (hereafter, “ADOA”), a biomass burning factor (“BBOA”), and a fossil-fuel  
225 hydrocarbon-like factor (“HOA”). Three factors interpreted as secondary production and



226 processing were resolved: a more-oxidized oxygenated factor (“MO-OOA”), a less-oxidized  
227 oxygenated factor (“LO-OOA”), and an isoprene epoxydiols-derived factor (“IEPOX-SOA”).

228 The HOA factor profile had characteristic ions of  $C_4H_7^+$  and  $C_4H_9^+$  at nominal values of  
229  $m/z$  55 and 57, respectively (Figure 4a). It had an oxygen-to-carbon (O:C) ratio of  $0.18 \pm 0.02$ ,  
230 the lowest among the six factors (Table 1). In line with the AMS PMF literature, the HOA factor  
231 represents a class of primary hydrocarbon-like organic compounds that are typically associated  
232 with traffic emissions (Zhang et al., 2005). In the present study, the HOA factor loadings  
233 accounted for 6% of the organic mass concentrations on average (Figure 4a, inset). As a point of  
234 comparison, the average in the southeastern USA typically varies from 9% to 15% (Xu et al.,  
235 2015b). The lower relative contribution of 6% in this study might in part be due to a larger  
236 relative role of secondary production in the environment of a tropical forest. In addition, the  
237 distance from Manaus to the T3 site might allow time for substantial vertical mixing, dilution,  
238 and subsequent evaporation of primary emissions into entrained background air (Robinson et al.,  
239 2007; Liu et al., accepted; Shilling et al., in preparation). Finally, the possible differences in  
240 emission profiles associated with different types of regional economic development between the  
241 Brazilian Amazon and USA (e.g., fleet density, fuel matrix, industry, and so forth) should also be  
242 considered. The HOA factor loading decreased during the day, which can be explained by the  
243 growth of the planetary boundary layer (PBL) and the subsequent dilution of the concentrations  
244 of primary emissions (Figure 4b). The time series of HOA factor loading did not correlate well  
245 ( $R < 0.5$ ) with any of the co-located measurements at T3 (Figure 5). It is plotted alongside the  
246 time series of  $NO_y$  concentration in Figure 4c.

247 The BBOA factor profile was characterized by distinct peaks of  $C_2H_4O_2^+$  ( $m/z$  60) and  
248  $C_3H_5O_2^+$  ( $m/z$  73), as shown in Figure 4a. These peaks can be attributed to levoglucosan and



249 other anhydrous sugars that result from biomass pyrolysis (Schneider et al., 2006; Cubison et al.,  
250 2011). Correlations of the factor loadings with the mass concentrations of levoglucosan and  
251 vanillin ( $R > 0.8$ ) measured by SV-TAG corroborate the association with biomass burning  
252 (Figure 4c). The BBOA factor of this study had an O:C ratio of  $0.61 \pm 0.08$  (Table 1), which is  
253 consistent with large contributions from levoglucosan (O:C of 0.83) and similar sugars. The  
254 factor loading on average accounted for 9% of the organic PM<sub>1</sub> mass concentration (Figure 4a,  
255 inset). This result is consistent with the low incidence of fires in the Amazon during the wet  
256 season (Martin et al., 2016). The BBOA factor loading typically decreased during the day  
257 (Figure 4b), which is suggestive of the dilution of local sources during the development of the  
258 PBL rather than long-range transport. Emissions from local fires around T3, including trash and  
259 tree burning, as well as from wood-fueled brick kilns along the road from Manaus to T3 might  
260 have contributed to this factor.

261 The ADOA factor profile, distinguished prominently by the  $C_7H_7^+$  ion at  $m/z$  91, also had  
262 characteristic ions of  $C_4H_7^+$  at  $m/z$  55 and  $C_3H_5^+$  at  $m/z$  41 (Figure 4a). A peak at  $m/z$  91 can arise  
263 from many sources, including biogenic and anthropogenic emissions (Ng et al., 2011b). In itself,  
264  $m/z$  91 therefore does not serve as a tracer for a specific source or process without consideration  
265 of the atmospheric context. Factors having a characteristic  $m/z$  91 peak (usually labeled “91fac”)  
266 typically have been associated with biogenic emissions (Robinson et al., 2011; Budisulistiorini et  
267 al., 2015; Chen et al., 2015; Riva et al., 2016). The ADOA factor profile of this study, however,  
268 more strongly resembles the mass spectra previously reported for PM emissions from cooking  
269 activities (Lanz et al., 2007; Mohr et al., 2012) than those from “91fac” (Section S1; Figure S5).  
270 The ratio of  $m/z$  55 to  $m/z$  57 of the ADOA factor was 4.1. This ratio lies in the range of 2 to 10  
271 reported for several factors representing primary cooking emissions and is well above the range



272 of 0.8 to 1.4 reported for factors associated with traffic emissions, i.e., HOA (Mohr et al., 2012  
273 and references therein; Hu et al., 2016). Even though the ADOA factor profile has a large  
274 contribution from non-oxygenated ions, similar to HOA and consistent with a dominance by  
275 primary emissions, it also contains considerable signal from oxygenated ions, resulting in a  
276 relatively higher O:C of  $0.40 \pm 0.05$  (Table 1). The factor loading on average accounted for 13%  
277 of the organic  $PM_{10}$  mass concentration (Figure 4a, inset). The factor loading decreased as the  
278 PBL developed during the day, consistent with dominant non-photochemical, primary sources  
279 (Figure 4b). Furthermore, there were increases, albeit small, in factor loading at 12:00 and 18:00  
280 (local time), suggestive of breakfast-time and lunch-time cooking activities in Manaus based on a  
281 transport time of 4 to 6 h between the city and the T3 site (Martin et al., 2016; Cirino et al.,  
282 submitted). Manaus typically has four rush-hour periods each day from 6:30 to 8:00, 12:00 to  
283 13:30, 16:30 to 18:30, and 21:00 to 22:00. Traffic peaking at these hours may therefore also have  
284 contributed to the ADOA factor. Correlations between factor loading and external measurements  
285 exceeded  $R = 0.5$  for many anthropogenic markers, including concentrations of aromatics (e.g.,  
286 benzene, toluene, and  $C_8$  and  $C_9$  species), carbon monoxide, particle count, and  $NO_y$  (Figure 4c,  
287 Figure 5). Contributions from secondary processes cannot be ruled out, and it is possible that PM  
288 production from anthropogenic VOCs might have also been captured in this factor. Overall, the  
289 ADOA factor was interpreted in the present study as an indicator of anthropogenic influence  
290 associated with several sources in Manaus, most importantly cooking and possibly traffic  
291 emissions.

292 The IEPOX-SOA factor profile had marker ions of  $C_4H_5^+$  ( $m/z$  53) and  $C_5H_6O^+$  ( $m/z$  82)  
293 (Figure 4a; Lin et al., 2012; Hu et al., 2015; de Sá et al., 2017). It had an O:C ratio of  $0.9 \pm 0.10$   
294 (Table 1). The factor loading on average accounted for 17% of the organic  $PM_{10}$  mass



295 concentration (Figure 4a, inset). There were high correlations ( $R > 0.8$ ) between factor loadings  
296 and concentrations of C<sub>5</sub>-alkenetriols and 2-methyltetrols, which are markers of IEPOX-derived  
297 PM, produced by the photo-oxidation of isoprene under HO<sub>2</sub>-dominant conditions (Surratt et al.,  
298 2010; Lin et al., 2012; Figure 4c). The increase in factor loading during daytime was consistent  
299 with a photochemical source (Figure 4b). There were also correlations between factor loadings  
300 and concentrations of sulfate and some acids, such as tricarballic acid (TCA; Figure 5), in  
301 agreement with the association of IEPOX-derived PM and sulfate/acidity observed in other  
302 studies (Budisulistiorini et al., 2013; Nguyen et al., 2014; Kuwata et al., 2015). Overall, this  
303 factor was therefore interpreted as representative of PM produced from isoprene photo-oxidation  
304 under HO<sub>2</sub>-dominant conditions. The effects of urban pollution on the loadings of this factor  
305 were the focus of a previous publication (de Sá et al., 2017).

306 The two remaining factors, LO-OOA and MO-OOA, were also associated with secondary  
307 atmospheric processes. The LO-OOA and MO-OOA factors had O:C ratios of  $0.72 \pm 0.10$  and  
308  $1.09 \pm 0.17$ , respectively. The LO-OOA factor was characterized by the greatest ratio of signal  
309 intensity of the C<sub>2</sub>H<sub>3</sub>O<sup>+</sup> ion ( $m/z$  43) to that of the CO<sub>2</sub><sup>+</sup> ion ( $m/z$  44) (Figure 4a) compared to all  
310 other factors. This factor is usually attributed to lower-generation, less-oxidized, higher-volatility  
311 secondary organic PM (Jimenez et al., 2009). By comparison, the MO-OOA factor profile had  
312 the strongest CO<sub>2</sub><sup>+</sup> ( $m/z$  44) peak among all factors (Figure 4a). This factor is usually attributed  
313 to higher-generation, more-oxidized, less-volatile secondary organic PM or extensively oxidized  
314 primary PM of any type that has resided in the atmosphere for several days or more (Jimenez et  
315 al., 2009).

316 The LO-OOA factor loading on average accounted for 25% of the organic PM<sub>1</sub> mass  
317 concentration (Figure 4a, inset). The factor loading correlated better with the estimated



318 concentrations of inorganic nitrate than with organic or total nitrate (Figure 5; Section S2 and  
319 Figure S6), which is consistent with the interpretation of the higher volatility associated with this  
320 factor (Jimenez et al., 2009; Zhang et al., 2011). The factor loading also correlated ( $R > 0.7$ ) with  
321 the concentrations of 2-methylglyceric acid and methyl-butyl-tricarboxylic acid (MBTCA),  
322 which are products of isoprene and monoterpene oxidation, respectively, under NO-dominant  
323 conditions (Figure 4c; Figure 5). The factor loading increased starting at 9:00 (local time) and  
324 peaked in the afternoon hours (Figure 4b). This diel trend, tied to the sunlight cycle, tracked the  
325 typical daily emission patterns of isoprene and monoterpenes from the surrounding forest  
326 (Yáñez-Serrano et al., 2015). The absence of a sharp decline at sunset and the higher variability  
327 at nighttime may also indicate a contribution by terpene ozonolysis. For these several reasons,  
328 the LO-OOA factor was interpreted herein as secondary organic PM produced mostly within  
329 several hours of observations by many possible pathways, including (i) the photo-oxidation of  
330 isoprene along non-IEPOX pathways, (ii) the photo-oxidation of terpenes and other biogenic  
331 VOCs along both HO<sub>2</sub>- and NO-dominant reaction pathways, (iii) the ozonolysis of terpenes, and  
332 (iv) the possible production of SOM from anthropogenic emissions from Manaus.

333         The MO-OOA factor loading on average accounted for 30% of the organic PM<sub>1</sub> mass  
334 concentration (Figure 4a, inset). The factor loading correlated ( $R > 0.7$ ) with the mass  
335 concentrations of several particle-phase carboxylic acids as well as the concentrations of sulfate,  
336 ammonium, and ozone (Figure 5). The time series of malic acid and ozone concentrations are  
337 shown alongside the MO-OOA factor loadings in Figure 4c. Malic acid is a highly oxidized  
338 compound (O:C of 1.25), which may have many different sources (Röhrh and Lammel, 2002; van  
339 Pinxteren et al., 2014). The MO-OOA factor loading increased starting at 8:00 (local time;  
340 sunrise was at 6:00) and peaked between 10:00 and 16:00, with a large variability in the factor



341 loadings in the afternoon hours among different days (Figure 4b). The afternoon increase and  
342 day-to-day variability were consistent with strong but variable photochemical processing leading  
343 to further oxidation of organic PM during the day, depending on daily weather. The high O:C of  
344  $1.09 \pm 0.17$  could also be indicative of production of PM from aromatic compounds emitted from  
345 Manaus (Chhabra et al., 2011; Lambe et al., 2011). Overall, this factor was interpreted to  
346 represent highly oxidized PM from multiple processes. Species initially associated with HOA,  
347 BBOA, ADOA, IEPOX-SOA, and LO-OOA factors may converge after sufficient atmospheric  
348 oxidation to become represented by the MO-OOA factor (Jimenez et al., 2009; Palm et al.,  
349 2018).

### 350 **3.3 Shifts in PM with anthropogenic influences**

#### 351 **3.3.1 Cluster Analysis**

352 To further investigate changes in the concentration and composition of PM associated  
353 with anthropogenic influences, a Fuzzy c-means (FCM) algorithm was applied to the time series  
354 of concentrations of particle number,  $\text{NO}_x$ , ozone, black carbon, and sulfate measurements at the  
355 T3 site (Bezdek et al., 1984). The analysis was fully independent of the PMF results. For each  
356 point in time, these concentrations represented the spatial coordinates of the data point. As  
357 discussed below, four clusters were identified. Based on measures of spatial similarity, the  
358 clustering algorithm attributed to each data point a degree of membership relative to each of the  
359 four clusters (Section S3; Figure S7 and Figure S8).

360 The scope of the clustering analysis was restricted to afternoon time points for which ten-  
361 hour air mass backtrajectories did not intersect significant precipitation and for which solar  
362 irradiance at T3 averaged over the previous 4 h was higher than  $200 \text{ W m}^{-2}$  (Section S3). This  
363 scope aimed at capturing fair-weather conditions and thereby minimizing the role of otherwise



364 confounding processes, such as boundary layer dynamics and wet deposition. The elimination of  
365 trajectories having precipitation, however, should not be regarded as fully accurate given the  
366 uncertainties in the HYSPLIT trajectories. The scoped dataset spanned 24 afternoons.

367 Four clusters were identified based on minimization of the FCM objective function as  
368 well as a subjective assessment of meaningful interpretation of the set of clusters (Section S3).  
369 The FCM algorithm returned a matrix containing the degrees of membership (ranging from 0 to  
370 1) to each of the four clusters (columns) for each point in time (rows). For any given time point  
371 (i.e., row), the sum of its degrees of membership to clusters (i.e., sum across columns) was  
372 always unity, by definition. A collection of examples, representing 37% of the analyzed data  
373 points by FCM, is shown in Figure 6a. For times predominantly associated with only one cluster  
374 (e.g., Feb 9 and Feb 10), the corresponding air mass backtrajectories are plotted in Figure 7. The  
375 FCM algorithm also returned the coordinates of cluster centroids, which are listed in Table 2.

376 Two clusters of data were interpreted as “background” and labeled “Bkgd-1” and “Bkgd-  
377 2”. They were characterized by  $\text{NO}_y < 1$  ppb, ozone  $< 20$  ppb, and particle number  $< 1200 \text{ cm}^{-3}$   
378 (Table 2; Figure 6). The two clusters differed especially in that Bkgd-2 had significantly larger  
379 concentrations of sulfate and black carbon. A comparison of the datasets of Feb 13  
380 (predominantly Bkgd-1) and Feb 16 (predominantly Bkgd-2) in Figure 6 highlights these  
381 differences. Concentrations of sulfate and black carbon were  $0.15$  and  $0.10 \mu\text{g m}^{-3}$ , respectively,  
382 on Feb 13, compared to  $0.40$  and  $0.15 \mu\text{g m}^{-3}$  on Feb 16. The backtrajectories associated with  
383 Bkgd-1 had both northeasterly and southeasterly components. The wind fields, out of line with  
384 the trade winds, may suggest passage through recent weather systems and may imply wet  
385 deposition, which in turn might explain lower gas and particle concentrations (Table 2). These  
386 recent weather systems might not have been excluded from the scoped dataset because of



387 inaccuracies in the intersections of the backtrajectories with precipitation data, as discussed  
388 above, or because they were more distant than captured by the 10-h backtrajectories. Consistent  
389 with this hypothesis, the centroid value calculated for the 4-h averaged solar irradiance at T3  
390 (Section 3.3.2) was lower for Bkgd-1 ( $400 \text{ W m}^{-2}$ ) compared to the other clusters ( $600 \text{ W m}^{-2}$ ),  
391 suggesting an association of Bkgd-1 with overcast conditions. By comparison, the  
392 backtrajectories associated with Bkgd-2 were predominantly from the northeast, coming from the  
393 direction of the T0t and T0a sites (Figure 7), in line with the dominant trade winds of the wet  
394 season. The air masses of Bkgd-2 may have experienced less wet deposition and may represent  
395 more extensive atmospheric oxidation than those of Bkgd-1. They may also have carried PM  
396 contributions from out-of-basin sources, which would be consistent with the higher sulfate and  
397 black carbon concentrations of Bkgd-2 compared to Bkgd-1 (Chen et al., 2009; Pöhlker et al.,  
398 2017).

399 Two other clusters were interpreted as “polluted” and labeled “Pol-1” and “Pol-2”. They  
400 were characterized by concentrations of  $\text{NO}_y > 1 \text{ ppb}$ , ozone  $> 20 \text{ ppb}$ , and particle number  $>$   
401  $1200 \text{ cm}^{-3}$  (Table 2; Figure 6). The dataset of the afternoon of Mar 9 illustrates a shift in  
402 dominance from Pol-2 to Pol-1 (Figure 6). Although Pol-1 and Pol-2 both have high  
403 concentrations of sulfate and other pollutants, they differ in the extent of those high  
404 concentrations. The explanation may be that these clusters represent different source regions.  
405 Pol-1 may be associated with emissions from the northern region of Manaus, and Pol-2 may be  
406 associated with emissions from the southern region of Manaus. Industry, power production, and  
407 oil refineries are concentrated in the southeastern region of Manaus (Figure S9; Medeiros et al.,  
408 2017). Population density and commercial activity is concentrated in the southwestern portion of  
409 the city where downtown is located (Figure S10). Aircraft observations show that concentrations



410 of sulfate as well as other pollutants are higher in the urban outflow from the southern compared  
411 to the northern region of Manaus (Figure S10). Directional plots of SO<sub>2</sub> and particle number  
412 concentrations observed at the T2 site further demonstrate the heterogeneity in Manaus  
413 emissions (Figure S10). This hypothesis of a geographical difference in source regions  
414 qualitatively aligns with the differences in backtrajectories characteristic of times dominated by  
415 Pol-1 and Pol-2 (Figure 7). This interpretation does imply, however, that the backtrajectories  
416 may have a 20° inaccuracy. Such inaccuracy is reasonable for the application of HYSPLIT  
417 modeling in this region given (i) the absence of surface weather stations and (ii) the relatively  
418 large scale of input wind fields (i.e., 50 km) compared to the scale of modeling (i.e., 70 km from  
419 T3 to Manaus and a city cross section of 20 km).

### 420 **3.3.2 Comparison of PM among clusters**

421 The characteristic PM composition associated with each cluster was determined by  
422 calculating the centroid coordinates of the clusters for the AMS species and PMF factors  
423 (Section S3). The centroid coordinate of a cluster for a given variable is defined as a weighted  
424 mean of that variable across all points in time, where the weight is the degree of membership of  
425 each data point to that cluster. A comparison of PM<sub>1</sub> concentrations and compositions for the  
426 four clusters is shown in Figure 8. Values are listed in Table 2.

427 The NR-PM<sub>1</sub> mass concentrations increased by 25% to 200% in clusters Pol-1 and Pol-2  
428 compared to clusters Bkgd-1 and Bkgd-2 (Figure 8a). Increases in sulfate and associated  
429 ammonium concentrations had a smaller yet non-negligible role in the increased PM<sub>1</sub> mass  
430 concentrations. Sources of sulfate other than Manaus sustain relatively high concentrations in the  
431 Amazon basin, as represented by the Bkgd-2 cluster (Chen et al., 2009; de Sá et al., 2017).  
432 Compared to these regional background concentrations (i.e., Bkgd-2 cluster), the increases in



433 sulfate concentrations were significant only for air masses associated with the heavily  
434 industrialized and densely populated southern region of Manaus (i.e., Pol-2 cluster).

435         With respect to the composition of the organic PM, Figure 8b shows that the Bkgd-1  
436 cluster had large contribution from the LO-OOA factor. By comparison, the Bkgd-2 cluster had  
437 larger contributions from the MO-OOA and IEPOX-SOA factors. A comparison of 13 Feb and  
438 16 Feb of 2014 (Figure 6d) illustrates these findings. The low mass concentrations and the  
439 dominant contribution by the LO-OOA factor suggest that the Bkgd-1 cluster may represent  
440 conditions under which secondary organic PM was produced within recent hours through photo-  
441 oxidation of VOCs emitted by the forest and subsequent condensation of secondary organic  
442 material. The low sulfate concentrations for Bkgd-1 may rationalize the absence of a significant  
443 contribution by the IEPOX-SOA factor. Isoprene photo-oxidation may have contributed to PM  
444 production by pathways other than IEPOX uptake (Krechmer et al., 2015; Riva et al., 2016). By  
445 comparison, for Bkgd-2, the higher mass concentrations and the greater contributions by IEPOX-  
446 SOA and MO-OOA factors suggest that this cluster may represent conditions under which  
447 secondary organic PM was a combination of material produced both on that day as well as on  
448 previous days. During transport, the organic PM may have undergone extensive atmospheric  
449 oxidation by a combination of surface and condensed-phase chemistry, including cloud water  
450 processes (Carlton et al., 2006; Ervens et al., 2011; Hoyle et al., 2011; Perraud et al., 2012).  
451 Concentrations and composition of the Bkgd-2 cluster may therefore represent an extensive  
452 geographical footprint.

453         The organic PM concentration and composition associated with the Pol-1 and Pol-2  
454 clusters were distinct from those of the Bkgd-1 and Bkgd-2 clusters (Figure 8). The mass  
455 concentrations of organic PM were greater by 25% to 150% for Pol-1 and Pol-2. According to



456 the PMF factors (Figure 8b), the larger part of this increase in organic PM between the  
457 background and polluted clusters was tied to the production of secondary organic PM, although  
458 primary emissions also contributed significantly. By comparison, for both Bkgd-1 and Bkgd-2  
459 clusters, contributions by primary emissions were negligible, as indicated by the low summed  
460 contribution of factors of primary origin (i.e., ADOA, BBOA, and HOA) to the organic PM<sub>1</sub> (<  
461 10%). For Pol-1 and Pol-2, the ADOA factor loading on average accounted for 10% of the  
462 organic mass concentration at T3, serving as a strong marker of Manaus pollution. A comparison  
463 of 9 Feb and 9 Mar with 13 Feb and 16 Feb illustrates these findings (Figure 6d).

464 In regard to secondary organic PM, the IEPOX-SOA factor loading decreased by almost  
465 50% under polluted compared to background conditions. de Sá et al. (2017) attributed this  
466 decrease to the suppression of IEPOX production by elevated NO concentrations. This  
467 suppression typically outweighed possible enhancements in IEPOX uptake and subsequent PM  
468 production because of elevated sulfate concentrations. By contrast, the LO-OOA and MO-OOA  
469 factor loadings increased by 50% to 100% under polluted conditions. These increases exceeded  
470 the decrease in IEPOX-SOA factor loadings, resulting in a net increase of around 100% in mass  
471 concentration of secondary organic PM (Figure 8).

472 The shifts in the processes governing the production of secondary organic PM because of  
473 increased NO<sub>x</sub>, OH, and O<sub>3</sub> concentrations characteristic of the pollution plume were complex  
474 and non-linear (Figure 9a). Overall, the oxidation pathways were driven faster. The relatively  
475 high  $f_{\text{CO}_2^+}$  values and O:C ratios of all factors (Table 1), including those associated with primary  
476 emissions, compared to typical values at other locations worldwide (Canagaratna et al., 2015),  
477 corroborate this interpretation. Ozone concentrations in the plume increase by 200 to 300 %, and  
478 hydroxyl radical concentrations increased by 250% or more (Liu et al., accepted). As HO<sub>2</sub>-



479 dominant pathways were inhibited, NO-dominant pathways became active. Increased oxidant  
480 concentrations may also have promoted additional multigenerational chemistry of semi- or  
481 intermediate-volatility species (Robinson et al., 2007). Oxidation of VOCs by aqueous-phase  
482 reactions, including in-cloud processing, and oxidation of biomass burning emissions may also  
483 have played roles to varying degrees on different days (Carlton et al., 2006; Ervens et al., 2011;  
484 Hoyle et al., 2011; Perraud et al., 2012). In addition, when primary and secondary PM mass  
485 concentrations increased, further uptake of oxidized semi-volatile molecules could have been  
486 thermodynamically favored according to partitioning theory, representing a positive feedback on  
487 the increase of mass concentrations (Pankow, 1994; Odum et al., 1996; Carlton et al., 2010).

488         The increase in the LO-OOA and MO-OOA factor loadings associated with Pol-1 and  
489 Pol-2 indicates that the net effect of this accelerated and modified chemistry was the quick  
490 production and further oxidation of secondary organic PM. Precursors may have included both  
491 the wide range of biogenic VOCs as well as contributions from anthropogenic precursors, such  
492 as gas-phase species from vehicle emissions or evaporated primary material (Nordin et al., 2013;  
493 Presto et al., 2014). The LO-OOA factor loading was important for the polluted conditions of  
494 Pol-1 and Pol-2 as well as for the clean conditions of Bkgd-1. This result is not necessarily  
495 because of an in-common molecular composition but rather because of an in-common process,  
496 i.e., fresh production of secondary organic PM (Figure 9b). Likewise, the MO-OOA factor  
497 loading was important for Pol-1, Pol-2, and Bkgd-2 because this factor represented an in-  
498 common process, i.e., extensive oxidation (Figure 9b). In the case of the MO-OOA factor, there  
499 is also an overall in-common composition characterized by highly oxidized species even as  
500 precursor species and subsequent oxidation pathways differed (Jimenez et al., 2009).



501           The complexity of the real atmospheric processes, as illustrated in Figure 9, is to some  
502 extent captured by the instrumental and analytical tools herein employed. Positive-matrix  
503 factorization identified several broad classes of organic PM. Some PMF factors had sufficiently  
504 unique signatures that they could be associated to one specific source and/or process (e.g., HOA  
505 and IEPOX-SOA). Other factors, in contrast, represented a wide range of sources that shared in-  
506 common processes (e.g., LO-OOA and MO-OOA). The clustering analysis contextualized the  
507 PMF results and demonstrated that the effects of the urban pollution were neither limited to nor  
508 captured by a single PMF factor. Instead, the urban plume influenced several PMF factors in  
509 different ways and to different extents. The implication is that changes in the AMS spectral  
510 signature of the organic PM caused by polluted conditions may not be sufficiently unique to  
511 allow for its complete separation by PMF analysis alone, especially in respect to the production  
512 of secondary organic PM. In this context, the Fuzzy c-means analysis served herein as a useful  
513 tool to incorporate auxiliary datasets and thereby to further understand anthropogenic influences  
514 on PM production and characteristics.

#### 515 **4. Summary and conclusions**

516           Changes in the concentrations and the composition of fine-mode PM due to the influence  
517 of anthropogenic emissions were investigated for the Amazonian wet season. Organic material  
518 dominated the submicron composition, consistently representing between 70% and 80% of the  
519  $PM_{10}$  mean mass concentration across measurement sites upwind and downwind of Manaus and  
520 across different levels of pollution. Absolute mass concentrations, however, varied significantly  
521 among sites. Average concentrations downwind of Manaus were 100% to 200% higher than  
522 those upwind. Furthest downwind at T3, the organic component was more oxidized compared to  
523 that at the T2 site.



524 Positive-matrix factorization and Fuzzy c-means clustering were applied to the datasets to  
525 obtain a composite analysis of the shifts in PM<sub>1</sub> concentrations and composition under polluted  
526 conditions. Based on the FCM clustering, every point in time at T3 was interpreted as being  
527 affected by a combination of four influences, as represented by four clusters. Two background  
528 (Bkgd-1 and Bkgd-2) and two polluted (Pol-1 and Pol-2) clusters were identified. Particle mass  
529 concentrations were double for polluted compared to background conditions. Contributions from  
530 secondary processes dominated (> 80%) for both background and polluted conditions.

531 In terms of primary emissions, absolute contributions increased by a factor of five or  
532 more under polluted conditions, corresponding to an increase from < 10% to 15% of total PM<sub>1</sub>.  
533 The ADOA factor loading increased over five-fold for the polluted compared to the background  
534 clusters, and this factor thus served as a strong tracer of Manaus pollution. BBOA and HOA  
535 factor loadings, associated with biomass burning and fossil fuels, respectively, increased by two-  
536 fold with pollution. The ADOA factor loading represented 61% to 76% of the total primary  
537 factor loadings for the Pol-1 and Pol-2 clusters.

538 As for the secondary processes, the analysis further finds that the pollution plume acted  
539 both to shift pathways of secondary organic PM production and to accelerate the atmospheric  
540 oxidation of pre-existing organic PM. The oxidation of biogenic PM precursors shifted from  
541 HO<sub>2</sub>- to NO-dominant pathways, and the oxidation of anthropogenic precursors possibly  
542 contributed to increased PM concentrations. The IEPOX-SOA factor loadings were highest for  
543 the Bkgd-2 cluster, associated with long-range transport under background conditions, and  
544 decreased by almost 50% for the polluted clusters, in line with a shift of isoprene oxidation from  
545 HO<sub>2</sub>- to NO-dominant pathways. Concomitantly, the LO-OOA factor loading increased by more  
546 than 50% for these clusters, suggesting rapid in-plume production of secondary organic PM



547 through several pathways. The LO-OOA factor was also important for the Bkgd-1 cluster,  
548 associated with fresh background conditions, which is suggestive of recent biogenic organic PM  
549 production. The MO-OOA factor had large relative contributions in the Bkgd-2, Pol-1, and Pol-2  
550 clusters, suggestive of significant oxidative processing associated with these clusters. Increases  
551 of up to 300% in the MO-OOA factor loadings for Pol-1 and Pol-2 relative to background  
552 conditions of Bkgd-1 showed the effects of an accelerated oxidation cycle, leading to highly  
553 oxidized PM downwind of Manaus. Based on this and related studies (Liu et al., 2016b; de Sá et  
554 al., 2017; Martin et al., 2017), the critical lever seems to be increased concentrations of nitrogen  
555 oxides in the pollution plume for both directly shifting and indirectly accelerating mechanisms of  
556 secondary organic PM production in central Amazonia during the wet season.

557       The altered composition under anthropogenic influences also affects the physical  
558 properties of the PM<sub>1</sub>. Bateman et al. (2017), using the results of the PMF analysis presented  
559 herein, reported a shift from predominantly liquid PM under background conditions to a  
560 considerable presence of non-liquid PM above 50% RH under polluted conditions. Non-liquid  
561 PM can have different reactive chemistry from liquid PM (Li et al., 2015; Liu et al., 2018). A  
562 linear relationship between the increase in particle rebound fraction and the sum of ADOA,  
563 BBOA, and HOA factor loadings had an  $R^2$  of 0.7. The highest individual correlation was with  
564 the ADOA factor loading (Bateman, personal communication). In addition, Thalman et al.  
565 (2017), also using the PMF results reported herein, concluded that the larger relative contribution  
566 of secondary organic material during the daytime compared to the nighttime was the primary  
567 driver of the diel trend of higher particle hygroscopicity during the day compared to the night, as  
568 tied to cloud condensation nuclei (CCN) properties.



569            This study communicates a snapshot of the changes that occur in the atmospheric  
570 composition over a tropical forest because of regional urbanization. In the context of a forest in  
571 transition (Davidson et al., 2012), the findings herein provide a quantitative assessment of the  
572 effects of urban pollution on the forested surroundings of Manaus. The studied region and the  
573 observed changes in atmospheric composition represent a microcosm that might become more  
574 widespread through Amazonia as urbanization trends continue in the future. Further  
575 investigations of the specific chemical pathways and physical mechanisms that enhance PM  
576 production in the urban plume are warranted to understand what other pollutants are critical for  
577 control in the context of ongoing and future air quality regulation in the study region as well as  
578 for other tropical forested environments worldwide.



**Acknowledgments.** Institutional support was provided by the Central Office of the Large Scale Biosphere Atmosphere Experiment in Amazonia (LBA), the National Institute of Amazonian Research (INPA), and Amazonas State University (UEA). We acknowledge support from the Atmospheric Radiation Measurement (ARM) Climate Research Facility, a user facility of the United States Department of Energy (DOE, DE-SC0006680), Office of Science, sponsored by the Office of Biological and Environmental Research, and support from the Atmospheric System Research (ASR, DE-SC0011115, DE-SC0011105) program of that office. Additional funding was provided by the Amazonas State Research Foundation (FAPEAM 062.00568/2014 and 134/2016), the São Paulo State Research Foundation (FAPESP 2013/05014-0), the USA National Science Foundation (1106400 and 1332998), and the Brazilian Scientific Mobility Program (CsF/CAPES). S. S. de Sá acknowledges support by the Faculty for the Future Fellowship of the Schlumberger Foundation. BBP is grateful for a US EPA STAR Graduate Fellowship (FP-91761701-0). The authors thank Paulo Castillo for his assistance in quality-checking the black carbon data from MAOS. Data access from the Sistema de Proteção da Amazônia (SIPAM) is gratefully acknowledged. The research was conducted under scientific license 001030/2012-4 of the Brazilian National Council for Scientific and Technological Development (CNPq).



## References

- Andreae, M. O., Acevedo, O. C., Araùjo, A., Artaxo, P., Barbosa, C. G. G., Barbosa, H. M. J., Brito, J., Carbone, S., Chi, X., Cintra, B. B. L., da Silva, N. F., Dias, N. L., Dias-Júnior, C. Q., Ditas, F., Ditz, R., Godoi, A. F. L., Godoi, R. H. M., Heimann, M., Hoffmann, T., Kesselmeier, J., Könemann, T., Krüger, M. L., Lavric, J. V., Manzi, A. O., Lopes, A. P., Martins, D. L., Mikhailov, E. F., Moran-Zuloaga, D., Nelson, B. W., Nölscher, A. C., Santos Nogueira, D., Piedade, M. T. F., Pöhlker, C., Pöschl, U., Quesada, C. A., Rizzo, L. V., Ro, C. U., Ruckteschler, N., Sá, L. D. A., de Oliveira Sá, M., Sales, C. B., dos Santos, R. M. N., Saturno, J., Schöngart, J., Sörgel, M., de Souza, C. M., de Souza, R. A. F., Su, H., Targhetta, N., Tóta, J., Trebs, I., Trumbore, S., van Eijck, A., Walter, D., Wang, Z., Weber, B., Williams, J., Winderlich, J., Wittmann, F., Wolff, S., and Yáñez-Serrano, A. M.: The Amazon Tall Tower Observatory (ATTO): overview of pilot measurements on ecosystem ecology, meteorology, trace gases, and aerosols, *Atmos. Chem. Phys.*, **15**, 10723-10776, 2015, [10.5194/acp-15-10723-2015](https://doi.org/10.5194/acp-15-10723-2015).
- Artaxo, P., Rizzo, L. V., Brito, J. F., Barbosa, H. M. J., Arana, A., Sena, E. T., Cirino, G. G., Bastos, W., Martin, S. T., and Andreae, M. O.: Atmospheric aerosols in Amazonia and land use change: from natural biogenic to biomass burning conditions, *Faraday Disc.*, **165**, 203-235, 2013, [10.1039/C3FD00052D](https://doi.org/10.1039/C3FD00052D).
- Bateman, A. P., Gong, Z., Harder, T. H., de Sá, S. S., Wang, B., Castillo, P., China, S., Liu, Y., O'Brien, R. E., Palm, B. B., Shiu, H. W., Cirino, G. G., Thalman, R., Adachi, K., Alexander, M. L., Artaxo, P., Bertram, A. K., Buseck, P. R., Gilles, M. K., Jimenez, J. L., Laskin, A., Manzi, A. O., Sedlacek, A., Souza, R. A. F., Wang, J., Zaveri, R., and Martin, S. T.: Anthropogenic influences on the physical state of submicron particulate matter over a tropical forest, *Atmos. Chem. Phys.*, **17**, 1759-1773, 2017, [10.5194/acp-17-1759-2017](https://doi.org/10.5194/acp-17-1759-2017).
- Bezdek, J. C., Ehrlich, R., and Full, W.: FCM: The fuzzy c-means clustering algorithm, *Computers & Geosciences*, **10**, 191-203, 1984.
- Brito, J., Carbone, S., de Sá, S. S., Martin, S. T., and Artaxo, P., in preparation.
- Budisulistiorini, S. H., Canagaratna, M. R., Croteau, P. L., Marth, W. J., Baumann, K., Edgerton, E. S., Shaw, S. L., Knipping, E. M., Worsnop, D. R., Jayne, J. T., Gold, A., and Surratt, J. D.: Real-time continuous characterization of secondary organic aerosol derived from isoprene epoxydiols in downtown Atlanta, Georgia, using the Aerodyne Aerosol Chemical Speciation Monitor, *Environ. Sci. Technol.*, **47**, 5686-5694, 2013, [10.1021/es400023n](https://doi.org/10.1021/es400023n).
- Budisulistiorini, S. H., Li, X., Bairai, S. T., Renfro, J., Liu, Y., Liu, Y. J., McKinney, K. A., Martin, S. T., McNeill, V. F., Pye, H. O. T., Nenes, A., Neff, M. E., Stone, E. A., Mueller, S., Knote, C., Shaw, S. L., Zhang, Z., Gold, A., and Surratt, J. D.: Examining the effects of anthropogenic emissions on isoprene-derived secondary organic aerosol formation during the 2013 Southern Oxidant and Aerosol Study (SOAS) at the Look Rock, Tennessee ground site, *Atmos. Chem. Phys.*, **15**, 8871-8888, 2015, [10.5194/acp-15-8871-2015](https://doi.org/10.5194/acp-15-8871-2015).



- Canagaratna, M. R., Jayne, J. T., Jimenez, J. L., Allan, J. D., Alfarra, M. R., Zhang, Q., Onasch, T. B., Drewnick, F., Coe, H., Middlebrook, A., Delia, A., Williams, L. R., Trimborn, A. M., Northway, M. J., DeCarlo, P. F., Kolb, C. E., Davidovits, P., and Worsnop, D. R.: Chemical and microphysical characterization of ambient aerosols with the aerodyne aerosol mass spectrometer, *Mass Spectrom. Rev.*, 26, 185-222, 2007, 10.1002/mas.20115.
- Canagaratna, M. R., Jimenez, J. L., Kroll, J. H., Chen, Q., Kessler, S. H., Massoli, P., Hildebrandt Ruiz, L., Fortner, E., Williams, L. R., Wilson, K. R., Surratt, J. D., Donahue, N. M., Jayne, J. T., and Worsnop, D. R.: Elemental ratio measurements of organic compounds using aerosol mass spectrometry: characterization, improved calibration, and implications, *Atmos. Chem. Phys.*, 15, 253-272, 2015, 10.5194/acp-15-253-2015.
- Cappa, C. D., Lack, D. A., Burkholder, J. B., and Ravishankara, A. R.: Bias in filter-based aerosol light absorption measurements due to organic aerosol loading: evidence from laboratory Measurements, *Aerosol Sci Technol*, 42, 1022-1032, 2008, 10.1080/02786820802389285.
- Carbone, S., Brito, J., De Sá, S. S., Martin, S. T., and Artaxo, P., in preparation.
- Carlton, A. G., Turpin, B. J., Lim, H.-J., Altieri, K. E., and Seitzinger, S.: Link between isoprene and secondary organic aerosol (SOA): Pyruvic acid oxidation yields low volatility organic acids in clouds, *Geophys. Res. Lett.*, 33, L06822, 2006, 10.1029/2005GL025374.
- Carlton, A. G., Pinder, R. W., Bhave, P. V., and Pouliot, G. A.: To What Extent Can Biogenic SOA be Controlled?, *Environ. Sci. Technol.*, 44, 3376-3380, 2010, 10.1021/es903506b.
- Chen, Q., Farmer, D. K., Schneider, J., Zorn, S. R., Heald, C. L., Karl, T. G., Guenther, A., Allan, J. D., Robinson, N., Coe, H., Kimmel, J. R., Pauliquevis, T., Borrmann, S., Pöschl, U., Andreae, M. O., Artaxo, P., Jimenez, J. L., and Martin, S. T.: Mass spectral characterization of submicron biogenic organic particles in the Amazon Basin, *Geophys. Res. Lett.*, 36, L20806, 2009, 10.1029/2009GL039880.
- Chen, Q., Farmer, D. K., Rizzo, L. V., Pauliquevis, T., Kuwata, M., Karl, T. G., Guenther, A., Allan, J. D., Coe, H., Andreae, M. O., Pöschl, U., Jimenez, J. L., Artaxo, P., and Martin, S. T.: Submicron particle mass concentrations and sources in the Amazonian wet season (AMAZE-08), *Atmos. Chem. Phys.*, 15, 3687-3701, 2015, 10.5194/acp-15-3687-2015.
- Chhabra, P., Ng, N., Canagaratna, M., Corrigan, A., Russell, L., Worsnop, D., Flagan, R., and Seinfeld, J.: Elemental composition and oxidation of chamber organic aerosol, *Atmos. Chem. Phys.*, 11, 8827-8845, 2011.
- Cirino, G. G., Brito, J., Barbosa, H. J. M., Rizzo, L. V., Carbone, S., de Sá, S. S., Tunved, P., Jimenez, J., Palm, B. B., Souza, R., Lavric, J., Tota, J., Oliveira, M., Wolff, S., Martin, S. T., and Artaxo, P.: Ground site observations of Manaus city plume evolution in GoAmazon2014/5, *Atmos Environ*, submitted.
- Cubison, M. J., Ortega, A. M., Hayes, P. L., Farmer, D. K., Day, D., Lechner, M. J., Brune, W. H., Apel, E., Diskin, G. S., Fisher, J. A., Fuelberg, H. E., Hecobian, A., Knapp, D. J., Mikoviny, T., Riemer, D., Sachse, G. W., Sessions, W., Weber, R. J., Weinheimer, A. J., Wisthaler, A., and Jimenez, J. L.: Effects of aging on organic aerosol from open biomass burning smoke in aircraft and laboratory studies, *Atmos. Chem. Phys.*, 11, 12049-12064, 2011, 10.5194/acp-11-12049-2011.
- Davidson, E. A., de Araújo, A. C., Artaxo, P., Balch, J. K., Brown, I. F., Bustamante, M. M., Coe, M. T., DeFries, R. S., Keller, M., and Longo, M.: The Amazon basin in transition, *Nature*, 481, 321-328, 2012.



- De Gouw, J. and Jimenez, J. L.: Organic Aerosols in the Earth's Atmosphere, *Environ. Sci. Technol.*, 43, 7614-7618, 2009, 10.1021/es9006004.
- de Gouw, J. A., Middlebrook, A. M., Warneke, C., Goldan, P. D., Kuster, W. C., Roberts, J. M., Fehsenfeld, F. C., Worsnop, D. R., Canagaratna, M. R., Pszenny, A. A. P., Keene, W. C., Marchewka, M., Bertman, S. B., and Bates, T. S.: Budget of organic carbon in a polluted atmosphere: Results from the New England Air Quality Study in 2002, *J. Geophys. Res. Atmos.*, 110, D16305, 2005, 10.1029/2004JD005623.
- de Gouw, J. A., Brock, C. A., Atlas, E. L., Bates, T. S., Fehsenfeld, F. C., Goldan, P. D., Holloway, J. S., Kuster, W. C., Lerner, B. M., Matthew, B. M., Middlebrook, A. M., Onasch, T. B., Peltier, R. E., Quinn, P. K., Senff, C. J., Stohl, A., Sullivan, A. P., Trainer, M., Warneke, C., Weber, R. J., and Williams, E. J.: Sources of particulate matter in the northeastern United States in summer: 1. Direct emissions and secondary formation of organic matter in urban plumes, *J. Geophys. Res. Atmos.*, 113, D08301, 2008, 10.1029/2007JD009243.
- de Sá, S. S., Palm, B. B., Campuzano-Jost, P., Day, D. A., Newburn, M. K., Hu, W., Isaacman-VanWertz, G., Yee, L. D., Thalman, R., Brito, J., Carbone, S., Artaxo, P., Goldstein, A. H., Manzi, A. O., Souza, R. A. F., Mei, F., Shilling, J. E., Springston, S. R., Wang, J., Surratt, J. D., Alexander, M. L., Jimenez, J. L., and Martin, S. T.: Influence of urban pollution on the production of organic particulate matter from isoprene epoxydiols in central Amazonia, *Atmos. Chem. Phys.*, 17, 6611-6629, 2017, 10.5194/acp-17-6611-2017.
- de Sá, S. S., Wernis, R., Palm, B. B., Yee, L. D., Isaacman-vanWertz, G., and Martin, S. T., in preparation.
- DeCarlo, P. F., Kimmel, J. R., Trimborn, A., Northway, M. J., Jayne, J. T., Aiken, A. C., Gonin, M., Fuhrer, K., Horvath, T., Docherty, K. S., Worsnop, D. R., and Jimenez, J. L.: Field-deployable, high-resolution, time-of-flight aerosol mass spectrometer, *Anal. Chem.*, 78, 8281-8289, 2006, 10.1021/ac061249n.
- dos Santos, M. J., Silva Dias, M. A. F., and Freitas, E. D.: Influence of local circulations on wind, moisture, and precipitation close to Manaus City, Amazon Region, Brazil, *J. Geophys. Res. Atmos.*, 119, 13,233-213,249, 2014, 10.1002/2014JD021969.
- Draxler, R. and Hess, G.: An overview of the HYSPLIT\_4 modeling system for trajectories, dispersion, and deposition, *Aust. Met. Mag.*, 47, 295-308, 1998.
- Ervens, B., Turpin, B., and Weber, R.: Secondary organic aerosol formation in cloud droplets and aqueous particles (aqSOA): a review of laboratory, field and model studies, *Atmos. Chem. Phys.*, 11, 11069-11102, 2011, 10.5194/acp-11-11069-2011.
- Farmer, D. K., Matsunaga, A., Docherty, K. S., Surratt, J. D., Seinfeld, J. H., Ziemann, P. J., and Jimenez, J. L.: Response of an aerosol mass spectrometer to organonitrates and organosulfates and implications for atmospheric chemistry, *Proc. Natl. Acad. Sci. USA*, 107, 6670-6675, 2010, 10.1073/pnas.0912340107.
- Fry, J. L., Kiendler-Scharr, A., Rollins, A. W., Wooldridge, P. J., Brown, S. S., Fuchs, H., Dubé, W., Mensah, A., dal Maso, M., Tillmann, R., Dorn, H. P., Brauers, T., and Cohen, R. C.: Organic nitrate and secondary organic aerosol yield from NO<sub>3</sub> oxidation of β-pinene evaluated using a gas-phase kinetics/aerosol partitioning model, *Atmos. Chem. Phys.*, 9, 1431-1449, 2009, 10.5194/acp-9-1431-2009.
- Fry, J. L., Draper, D. C., Zarzana, K. J., Campuzano-Jost, P., Day, D. A., Jimenez, J. L., Brown, S. S., Cohen, R. C., Kaser, L., Hansel, A., Cappellin, L., Karl, T., Hodzic Roux, A.,



- Turnipseed, A., Cantrell, C., Lefer, B. L., and Grossberg, N.: Observations of gas- and aerosol-phase organic nitrates at BEACHON-RoMBAS 2011, *Atmos. Chem. Phys.*, 13, 8585-8605, 2013, [10.5194/acp-13-8585-2013](https://doi.org/10.5194/acp-13-8585-2013).
- Glasius, M. and Goldstein, A. H.: Recent discoveries and future challenges in atmospheric organic chemistry, *Environ. Sci. Technol.*, 50, 2754-2764, 2016, [10.1021/acs.est.5b05105](https://doi.org/10.1021/acs.est.5b05105).
- Goldstein, A. H., Koven, C. D., Heald, C. L., and Fung, I. Y.: Biogenic carbon and anthropogenic pollutants combine to form a cooling haze over the southeastern United States, *Proc. Natl Acad. Sci. USA*, 106, 8835-8840, 2009, [10.1073/pnas.0904128106](https://doi.org/10.1073/pnas.0904128106).
- Hallquist, M., Wenger, J. C., Baltensperger, U., Rudich, Y., Simpson, D., Claeys, M., Dommen, J., Donahue, N. M., George, C., Goldstein, A. H., Hamilton, J. F., Herrmann, H., Hoffmann, T., Iinuma, Y., Jang, M., Jenkin, M. E., Jimenez, J. L., Kiendler-Scharr, A., Maenhaut, W., McFiggans, G., Mentel, T. F., Monod, A., Prévôt, A. S. H., Seinfeld, J. H., Surratt, J. D., Szmigielski, R., and Wildt, J.: The formation, properties and impact of secondary organic aerosol: current and emerging issues, *Atmos. Chem. Phys.*, 9, 5155-5236, 2009, [10.5194/acp-9-5155-2009](https://doi.org/10.5194/acp-9-5155-2009).
- Heald, C. L., Coe, H., Jimenez, J. L., Weber, R. J., Bahreini, R., Middlebrook, A. M., Russell, L. M., Jolleys, M., Fu, T. M., Allan, J. D., Bower, K. N., Capes, G., Crosier, J., Morgan, W. T., Robinson, N. H., Williams, P. I., Cubison, M. J., DeCarlo, P. F., and Dunlea, E. J.: Exploring the vertical profile of atmospheric organic aerosol: comparing 17 aircraft field campaigns with a global model, *Atmos. Chem. Phys.*, 11, 12673-12696, 2011, [10.5194/acp-11-12673-2011](https://doi.org/10.5194/acp-11-12673-2011).
- Hou, A. Y., Kakar, R. K., Neeck, S., Azarbarzin, A. A., Kummerow, C. D., Kojima, M., Oki, R., Nakamura, K., and Iguchi, T.: The Global Precipitation Measurement mission, *Bull. Am. Meteorol. Soc.*, 95, 701-722, 2014, [10.1175/bams-d-13-00164.1](https://doi.org/10.1175/bams-d-13-00164.1).
- Hoyle, C. R., Myhre, G., Berntsen, T. K., and Isaksen, I. S. A.: Anthropogenic influence on SOA and the resulting radiative forcing, *Atmos. Chem. Phys.*, 9, 2715-2728, 2009, [10.5194/acp-9-2715-2009](https://doi.org/10.5194/acp-9-2715-2009).
- Hoyle, C. R., Boy, M., Donahue, N. M., Fry, J. L., Glasius, M., Guenther, A., Hallar, A. G., Huff Hartz, K., Petters, M. D., Petäjä, T., Rosenoern, T., and Sullivan, A. P.: A review of the anthropogenic influence on biogenic secondary organic aerosol, *Atmos. Chem. Phys.*, 11, 321-343, 2011, [10.5194/acp-11-321-2011](https://doi.org/10.5194/acp-11-321-2011).
- Hu, W., Hu, M., Hu, W., Jimenez, J. L., Yuan, B., Chen, W., Wang, M., Wu, Y., Chen, C., Wang, Z., Peng, J., Zeng, L., and Shao, M.: Chemical composition, sources, and aging process of submicron aerosols in Beijing: Contrast between summer and winter, *J. Geophys. Res. Atmos.*, 121, 1955-1977, 2016, [10.1002/2015JD024020](https://doi.org/10.1002/2015JD024020).
- Hu, W. W., Campuzano-Jost, P., Palm, B. B., Day, D. A., Ortega, A. M., Hayes, P. L., Krechmer, J. E., Chen, Q., Kuwata, M., Liu, Y. J., de Sá, S. S., McKinney, K., Martin, S. T., Hu, M., Budisulistiorini, S. H., Riva, M., Surratt, J. D., St. Clair, J. M., Isaacman-Van Wertz, G., Yee, L. D., Goldstein, A. H., Carbone, S., Brito, J., Artaxo, P., de Gouw, J. A., Koss, A., Wisthaler, A., Mikoviny, T., Karl, T., Kaser, L., Jud, W., Hansel, A., Docherty, K. S., Alexander, M. L., Robinson, N. H., Coe, H., Allan, J. D., Canagaratna, M. R., Paulot, F., and Jimenez, J. L.: Characterization of a real-time tracer for isoprene epoxydiols-derived secondary organic aerosol (IEPOX-SOA) from aerosol mass spectrometer measurements, *Atmos. Chem. Phys.*, 15, 11807-11833, 2015, [10.5194/acp-15-11807-2015](https://doi.org/10.5194/acp-15-11807-2015).



- Huang, R.-J., Zhang, Y., Bozzetti, C., Ho, K.-F., Cao, J.-J., Han, Y., Daellenbach, K. R., Slowik, J. G., Platt, S. M., Canonaco, F., Zotter, P., Wolf, R., Pieber, S. M., Bruns, E. A., Crippa, M., Ciarelli, G., Piazzalunga, A., Schwikowski, M., Abbaszade, G., Schnelle-Kreis, J., Zimmermann, R., An, Z., Szidat, S., Baltensperger, U., Haddad, I. E., and Prevot, A. S. H.: High secondary aerosol contribution to particulate pollution during haze events in China, *Nature*, 514, 218-222, 2014, [10.1038/nature13774](https://doi.org/10.1038/nature13774).
- Isaacman-VanWertz, G., Yee, L. D., Kreisberg, N. M., Wernis, R., Moss, J. A., Hering, S. V., de Sá, S. S., Martin, S. T., Alexander, M. L., Palm, B. B., Hu, W., Campuzano-Jost, P., Day, D. A., Jimenez, J. L., Riva, M., Surratt, J. D., Viegas, J., Manzi, A., Edgerton, E., Baumann, K., Souza, R., Artaxo, P., and Goldstein, A. H.: Ambient Gas-Particle Partitioning of Tracers for Biogenic Oxidation, *Environ. Sci. Technol.*, 9952-9962, 2016, [10.1021/acs.est.6b01674](https://doi.org/10.1021/acs.est.6b01674).
- Jimenez, J. L., Canagaratna, M. R., Donahue, N. M., Prevot, A. S. H., Zhang, Q., Kroll, J. H., DeCarlo, P. F., Allan, J. D., Coe, H., Ng, N. L., Aiken, A. C., Docherty, K. S., Ulbrich, I. M., Grieshop, A. P., Robinson, A. L., Duplissy, J., Smith, J. D., Wilson, K. R., Lanz, V. A., Hueglin, C., Sun, Y. L., Tian, J., Laaksonen, A., Raatikainen, T., Rautiainen, J., Vaattovaara, P., Ehn, M., Kulmala, M., Tomlinson, J. M., Collins, D. R., Cubison, M. J., Dunlea, J., Huffman, J. A., Onasch, T. B., Alfarra, M. R., Williams, P. I., Bower, K., Kondo, Y., Schneider, J., Drewnick, F., Borrmann, S., Weimer, S., Demerjian, K., Salcedo, D., Cottrell, L., Griffin, R., Takami, A., Miyoshi, T., Hatakeyama, S., Shimono, A., Sun, J. Y., Zhang, Y. M., Dzepina, K., Kimmel, J. R., Sueper, D., Jayne, J. T., Herndon, S. C., Trimborn, A. M., Williams, L. R., Wood, E. C., Middlebrook, A. M., Kolb, C. E., Baltensperger, U., and Worsnop, D. R.: Evolution of organic aerosols in the atmosphere, *Science*, 326, 1525-1529, 2009, [10.1126/science.1180353](https://doi.org/10.1126/science.1180353).
- Joss, J. and Waldvogel, A.: Ein Spektrograph für Niederschlagstropfen mit automatischer Auswertung, *Pure and Applied Geophysics*, 68, 240-246, 1967, [10.1007/BF00874898](https://doi.org/10.1007/BF00874898).
- Krechmer, J. E., Coggon, M. M., Massoli, P., Nguyen, T. B., Crounse, J. D., Hu, W., Day, D. A., Tyndall, G. S., Henze, D. K., Rivera-Rios, J. C., Nowak, J. B., Kimmel, J. R., Mauldin, R. L., Stark, H., Jayne, J. T., Sipilä, M., Junninen, H., Clair, J. M. S., Zhang, X., Feiner, P. A., Zhang, L., Miller, D. O., Brune, W. H., Keutsch, F. N., Wennberg, P. O., Seinfeld, J. H., Worsnop, D. R., Jimenez, J. L., and Canagaratna, M. R.: Formation of low volatility organic compounds and secondary organic aerosol from isoprene hydroxyhydroperoxide low-NO oxidation, *Environ. Sci. Technol.*, 49, 10330-10339, 2015, [10.1021/acs.est.5b02031](https://doi.org/10.1021/acs.est.5b02031).
- Kroll, J. H., Ng, N. L., Murphy, S. M., Flagan, R. C., and Seinfeld, J. H.: Secondary organic aerosol formation from isoprene photooxidation under high-NO<sub>x</sub> conditions, *Geophys. Res. Lett.*, 32, 2005, [10.1029/2005GL023637](https://doi.org/10.1029/2005GL023637).
- Kroll, J. H., Ng, N. L., Murphy, S. M., Flagan, R. C., and Seinfeld, J. H.: Secondary organic aerosol formation from isoprene photooxidation, *Environ. Sci. Technol.*, 40, 1869-1877, 2006, [10.1021/es0524301](https://doi.org/10.1021/es0524301).
- Kuhn, U., Ganzeveld, L., Thielmann, A., Dindorf, T., Schebeske, G., Welling, M., Sciare, J., Roberts, G., Meixner, F. X., Kesselmeier, J., Lelieveld, J., Kolle, O., Ciccioli, P., Lloyd, J., Trentmann, J., Artaxo, P., and Andreae, M. O.: Impact of Manaus City on the Amazon Green Ocean atmosphere: ozone production, precursor sensitivity and aerosol load, *Atmos. Chem. Phys.*, 10, 9251-9282, 2010, [10.5194/acp-10-9251-2010](https://doi.org/10.5194/acp-10-9251-2010).



- Kummerow, C., Barnes, W., Kozu, T., Shiue, J., and Simpson, J.: The Tropical Rainfall Measuring Mission (TRMM) sensor package, *J. Atmos. Ocea. Technol.*, 15, 809-817, 1998, [10.1175/1520-0426\(1998\)015<0809:ttrmmt>2.0.co;2](https://doi.org/10.1175/1520-0426(1998)015<0809:ttrmmt>2.0.co;2).
- Kuwata, M., Liu, Y., McKinney, K., and Martin, S. T.: Physical state and acidity of inorganic sulfate can regulate the production of secondary organic material from isoprene photooxidation products, *Phys. Chem. Chem. Phys.*, 17, 5670-5678, 2015, [10.1039/C4CP04942J](https://doi.org/10.1039/C4CP04942J).
- Lack, D. A., Cappa, C. D., Covert, D. S., Baynard, T., Massoli, P., Sierau, B., Bates, T. S., Quinn, P. K., Lovejoy, E. R., and Ravishankara, A. R.: Bias in filter-based aerosol light absorption measurements due to organic aerosol loading: evidence from ambient measurements, *Aerosol Sci Technol*, 42, 1033-1041, 2008, [10.1080/02786820802389277](https://doi.org/10.1080/02786820802389277).
- Lambe, A. T., Onasch, T. B., Massoli, P., Croasdale, D. R., Wright, J. P., Ahern, A. T., Williams, L. R., Worsnop, D. R., Brune, W. H., and Davidovits, P.: Laboratory studies of the chemical composition and cloud condensation nuclei (CCN) activity of secondary organic aerosol (SOA) and oxidized primary organic aerosol (OPOA), *Atmos. Chem. Phys.*, 11, 8913-8928, 2011, [10.5194/acp-11-8913-2011](https://doi.org/10.5194/acp-11-8913-2011).
- Lanz, V. A., Alfarra, M. R., Baltensperger, U., Buchmann, B., Hueglin, C., and Prévôt, A. S. H.: Source apportionment of submicron organic aerosols at an urban site by factor analytical modelling of aerosol mass spectra, *Atmos. Chem. Phys.*, 7, 1503-1522, 2007, [10.5194/acp-7-1503-2007](https://doi.org/10.5194/acp-7-1503-2007).
- Li, Y. J., Liu, P., Gong, Z., Wang, Y., Bateman, A. P., Bergoend, C., Bertram, A. K., and Martin, S. T.: Chemical reactivity and liquid/nonliquid states of secondary organic material, *Environ. Sci. Technol.*, 49, 13264-13274, 2015, [10.1021/acs.est.5b03392](https://doi.org/10.1021/acs.est.5b03392).
- Liao, J., Froyd, K. D., Murphy, D. M., Keutsch, F. N., Yu, G., Wennberg, P. O., St. Clair, J. M., Crouse, J. D., Wisthaler, A., Mikoviny, T., Jimenez, J. L., Campuzano-Jost, P., Day, D. A., Hu, W., Ryerson, T. B., Pollack, I. B., Peischl, J., Anderson, B. E., Ziemba, L. D., Blake, D. R., Meinardi, S., and Diskin, G.: Airborne measurements of organosulfates over the continental US, *J. Geophys. Res. Atmos.*, 120, 2990-3005, 2015, [10.1002/2014JD022378](https://doi.org/10.1002/2014JD022378).
- Lin, Y.-H., Zhang, Z., Docherty, K. S., Zhang, H., Budisulistiorini, S. H., Rubitschun, C. L., Shaw, S. L., Knipping, E. M., Edgerton, E. S., Kleindienst, T. E., Gold, A., and Surratt, J. D.: Isoprene epoxydiols as precursors to secondary organic aerosol formation: acid-catalyzed reactive uptake studies with authentic compounds, *Environ. Sci. Technol.*, 46, 250-258, 2012, [10.1021/es202554c](https://doi.org/10.1021/es202554c).
- Liu, J., D'Ambro, E. L., Lee, B. H., Lopez-Hilfiker, F. D., Zaveri, R. A., Rivera-Rios, J. C., Keutsch, F. N., Iyer, S., Kurten, T., Zhang, Z., Gold, A., Surratt, J. D., Shilling, J. E., and Thornton, J. A.: Efficient isoprene secondary organic aerosol formation from a non-IEPOX pathway, *Environ. Sci. Technol.*, 2016a, [10.1021/acs.est.6b01872](https://doi.org/10.1021/acs.est.6b01872).
- Liu, P., Li, Y. J., Wang, Y., Bateman, A. P., Zhang, Y., Gong, Z., Bertram, A. K., and Martin, S. T.: Highly viscous states affect the browning of atmospheric organic particulate matter, *ACS Cent Sci*, 2018, [10.1021/acscentsci.7b00452](https://doi.org/10.1021/acscentsci.7b00452).
- Liu, Y., Brito, J., Dorris, M. R., Rivera-Rios, J. C., Seco, R., Bates, K. H., Artaxo, P., Duvoisin, S., Keutsch, F. N., Kim, S., Goldstein, A. H., Guenther, A. B., Manzi, A. O., Souza, R. A. F., Springston, S. R., Watson, T. B., McKinney, K. A., and Martin, S. T.: Isoprene



- photochemistry over the Amazon rain forest, *Proc. Natl. Acad. Sci. USA*, 113, 6125-6130, 2016b, [10.1073/pnas.1524136113](https://doi.org/10.1073/pnas.1524136113).
- Liu, Y., Seco, R., Kim, S., Guenther, A. B., Goldstein, A. H., Keutsch, F. N., Springston, S. R., Watson, T. B., Artaxo, P., Souza, R. A. F., McKinney, K. A., and Martin, S. T.: Isoprene photo-oxidation products quantify the effect of pollution on hydroxyl radicals over Amazonia, *Science Advances*, accepted.
- Machado, L. A. T., Dias, M. A. F. S., Morales, C., Fisch, G., Vila, D., Albrecht, R., Goodman, S. J., Calheiros, A. J. P., Biscaro, T., Kummerow, C., Cohen, J., Fitzjarrald, D., Nascimento, E. L., Sakamoto, M. S., Cunningham, C., Chaboureau, J.-P., Petersen, W. A., Adams, D. K., Baldini, L., Angelis, C. F., Sapucci, L. F., Salio, P., Barbosa, H. M. J., Landulfo, E., Souza, R. A. F., Blakeslee, R. J., Bailey, J., Freitas, S., Lima, W. F. A., and Tokay, A.: The Chuva Project: how does convection vary across Brazil?, *Bull. Am. Meteorol. Soc.*, 95, 1365-1380, 2014, [10.1175/bams-d-13-00084.1](https://doi.org/10.1175/bams-d-13-00084.1).
- Martin, S. T., Andreae, M. O., Artaxo, P., Baumgardner, D., Chen, Q., Goldstein, A. H., Guenther, A., Heald, C. L., Mayol-Bracero, O. L., McMurry, P. H., Pauliquevis, T., Pöschl, U., Prather, K. A., Roberts, G. C., Saleska, S. R., Silva Dias, M. A., Spracklen, D. V., Swietlicki, E., and Trebs, I.: Sources and properties of Amazonian aerosol particles, *Rev. Geophys.*, 48, RG2012, 2010a, [10.1029/2008RG000280](https://doi.org/10.1029/2008RG000280).
- Martin, S. T., Andreae, M. O., Althausen, D., Artaxo, P., Baars, H., Borrmann, S., Chen, Q., Farmer, D. K., Guenther, A., Gunthe, S. S., Jimenez, J. L., Karl, T., Longo, K., Manzi, A., Müller, T., Pauliquevis, T., Petters, M. D., Prenni, A. J., Pöschl, U., Rizzo, L. V., Schneider, J., Smith, J. N., Swietlicki, E., Tota, J., Wang, J., Wiedensohler, A., and Zorn, S. R.: An overview of the Amazonian aerosol characterization experiment 2008 (AMAZE-08), *Atmos. Chem. Phys.*, 10, 11415-11438, 2010b, [10.5194/acp-10-11415-2010](https://doi.org/10.5194/acp-10-11415-2010).
- Martin, S. T., Artaxo, P., Machado, L. A. T., Manzi, A. O., Souza, R. A. F., Schumacher, C., Wang, J., Andreae, M. O., Barbosa, H. M. J., Fan, J., Fisch, G., Goldstein, A. H., Guenther, A., Jimenez, J. L., Pöschl, U., Silva Dias, M. A., Smith, J. N., and Wendisch, M.: Introduction: observations and modeling of the green ocean Amazon (GoAmazon2014/5), *Atmos. Chem. Phys.*, 16, 4785-4797, 2016, [10.5194/acp-16-4785-2016](https://doi.org/10.5194/acp-16-4785-2016).
- Martin, S. T., Artaxo, P., Machado, L., Manzi, A. O., Souza, R. A. F., Schumacher, C., Wang, J., Biscaro, T., Brito, J., Calheiros, A., Jardine, K., Medeiros, A., Portela, B., Sá, S. S. d., Adachi, K., Aiken, A. C., Albrecht, R., Alexander, L., Andreae, M. O., Barbosa, H. M. J., Buseck, P., Chand, D., Comstock, J. M., Day, D. A., Dubey, M., Fan, J., Fast, J., Fisch, G., Fortner, E., Giangrande, S., Gilles, M., Goldstein, A. H., Guenther, A., Hubbe, J., Jensen, M., Jimenez, J. L., Keutsch, F. N., Kim, S., Kuang, C., Laskin, A., McKinney, K., Mei, F., Miller, M., Nascimento, R., Pauliquevis, T., Pekour, M., Peres, J., Petäjä, T., Pöhlker, C., Pöschl, U., Rizzo, L., Schmid, B., Shilling, J. E., Dias, M. A. S., Smith, J. N., Tomlinson, J. M., Tóta, J., and Wendisch, M.: The Green Ocean Amazon Experiment (GoAmazon2014/5) observes pollution affecting gases, aerosols, clouds, and rainfall over the rain forest, *Bulletin of the American Meteorological Society*, 98, 981-997, 2017, [10.1175/bams-d-15-00221.1](https://doi.org/10.1175/bams-d-15-00221.1).
- Medeiros, A. S. S., Calderaro, G., Guimarães, P. C., Magalhaes, M. R., Morais, M. V. B., Rafee, S. A. A., Ribeiro, I. O., Andreoli, R. V., Martins, J. A., Martins, L. D., Martin, S. T., and



- Souza, R. A. F.: Power plant fuel switching and air quality in a tropical, forested environment, *Atmos. Chem. Phys.*, 17, 8987-8998, 2017, 10.5194/acp-17-8987-2017.
- Mohr, C., DeCarlo, P. F., Heringa, M. F., Chirico, R., Slowik, J. G., Richter, R., Reche, C., Alastuey, A., Querol, X., Seco, R., Peñuelas, J., Jiménez, J. L., Crippa, M., Zimmermann, R., Baltensperger, U., and Prévôt, A. S. H.: Identification and quantification of organic aerosol from cooking and other sources in Barcelona using aerosol mass spectrometer data, *Atmos. Chem. Phys.*, 12, 1649-1665, 2012, 10.5194/acp-12-1649-2012.
- Ng, N., Canagaratna, M., Jimenez, J., Chhabra, P., Seinfeld, J., and Worsnop, D.: Changes in organic aerosol composition with aging inferred from aerosol mass spectra, *Atmos. Chem. Phys.*, 11, 6465-6474, 2011a, 10.5194/acp-11-6465-2011.
- Ng, N. L., Canagaratna, M. R., Jimenez, J. L., Zhang, Q., Ulbrich, I. M., and Worsnop, D. R.: Real-time methods for estimating organic component mass concentrations from aerosol mass spectrometer data, *Environ. Sci. Technol.*, 45, 910-916, 2011b, 10.1021/es102951k.
- Nguyen, T. B., Coggon, M. M., Bates, K. H., Zhang, X., Schwantes, R. H., Schilling, K. A., Loza, C. L., Flagan, R. C., Wennberg, P. O., and Seinfeld, J. H.: Organic aerosol formation from the reactive uptake of isoprene epoxydiols (IEPOX) onto non-acidified inorganic seeds, *Atmos. Chem. Phys.*, 14, 3497-3510, 2014, 10.5194/acp-14-3497-2014.
- Nordin, E. Z., Eriksson, A. C., Roldin, P., Nilsson, P. T., Carlsson, J. E., Kajos, M. K., Hellén, H., Wittbom, C., Rissler, J., Löndahl, J., Swietlicki, E., Svenningsson, B., Bohgard, M., Kulmala, M., Hallquist, M., and Pagels, J. H.: Secondary organic aerosol formation from idling gasoline passenger vehicle emissions investigated in a smog chamber, *Atmos. Chem. Phys.*, 13, 6101-6116, 2013, 10.5194/acp-13-6101-2013.
- Odum, J. R., Hoffmann, T., Bowman, F., Collins, D., Flagan, R. C., and Seinfeld, J. H.: Gas/particle partitioning and secondary organic aerosol yields, *Environ. Sci. Technol.*, 30, 2580-2585, 1996, 10.1021/es950943+.
- Palm, B. B., de Sá, S. S., Day, D. A., Campuzano-Jost, P., Hu, W., Seco, R., Sjostedt, S. J., Park, J. H., Guenther, A. B., Kim, S., Brito, J., Wurm, F., Artaxo, P., Thalman, R., Wang, J., Yee, L. D., Wernis, R., Isaacman-VanWertz, G., Goldstein, A. H., Liu, Y., Springston, S. R., Souza, R., Newburn, M. K., Alexander, M. L., Martin, S. T., and Jimenez, J. L.: Secondary organic aerosol formation from ambient air in an oxidation flow reactor in central Amazonia, *Atmos. Chem. Phys.*, 18, 467-493, 2018, 10.5194/acp-18-467-2018.
- Pankow, J. F.: An absorption model of gas/particle partitioning of organic compounds in the atmosphere, *Atmos. Environ.*, 28, 185-188, 1994, 10.1016/1352-2310(94)90093-0.
- Paulot, F., Crouse, J. D., Kjaergaard, H. G., Kürten, A., Clair, J. M. S., Seinfeld, J. H., and Wennberg, P. O.: Unexpected epoxide formation in the gas-phase photooxidation of isoprene, *Science*, 325, 730-733, 2009, 10.1126/science.1172910.
- Perraud, V., Bruns, E. A., Ezell, M. J., Johnson, S. N., Yu, Y., Alexander, M. L., Zelenyuk, A., Imre, D., Chang, W. L., Dabdub, D., Pankow, J. F., and Finlayson-Pitts, B. J.: Nonequilibrium atmospheric secondary organic aerosol formation and growth, *Proc. Natl Acad. Sci. USA*, 109, 2836-2841, 2012, 10.1073/pnas.1119909109.
- Pöhlker, M. L., Ditas, F., Saturno, J., Klimach, T., Hrabě de Angelis, I., Araújo, A., Brito, J., Carbone, S., Cheng, Y., Chi, X., Ditz, R., Gunthe, S. S., Kandler, K., Kesselmeier, J., Könemann, T., Lavrič, J. V., Martin, S. T., Mikhailov, E., Moran-Zuloaga, D., Rizzo, L. V., Rose, D., Su, H., Thalman, R., Walter, D., Wang, J., Wolff, S., Barbosa, H. M. J., Artaxo, P., Andreae, M. O., Pöschl, U., and Pöhlker, C.: Long-term observations of cloud condensation nuclei in the Amazon rain forest – Part 2: Variability and characteristic



- differences under near-pristine, biomass burning, and long-range transport conditions, *Atmos. Chem. Phys. Discuss.*, 2017, 1-51, 2017, 10.5194/acp-2017-847.
- Presto, A. A., Gordon, T. D., and Robinson, A. L.: Primary to secondary organic aerosol: evolution of organic emissions from mobile combustion sources, *Atmos. Chem. Phys.*, 14, 5015-5036, 2014, 10.5194/acp-14-5015-2014.
- Riva, M., Budisulistiorini, S. H., Chen, Y., Zhang, Z., D'Ambro, E. L., Zhang, X., Gold, A., Turpin, B. J., Thornton, J. A., Canagaratna, M. R., and Surratt, J. D.: Chemical characterization of secondary organic aerosol from oxidation of isoprene hydroxyhydroperoxides, *Environ. Sci. Technol.*, 2016, 10.1021/acs.est.6b02511.
- Robinson, A. L., Donahue, N. M., Shrivastava, M. K., Weitkamp, E. A., Sage, A. M., Grieshop, A. P., Lane, T. E., Pierce, J. R., and Pandis, S. N.: Rethinking organic aerosols: semivolatile emissions and photochemical aging, *Science*, 315, 1259-1262, 2007, 10.1126/science.1133061.
- Robinson, N. H., Hamilton, J. F., Allan, J. D., Langford, B., Oram, D. E., Chen, Q., Docherty, K., Farmer, D. K., Jimenez, J. L., Ward, M. W., Hewitt, C. N., Barley, M. H., Jenkin, M. E., Rickard, A. R., Martin, S. T., McFiggans, G., and Coe, H.: Evidence for a significant proportion of Secondary Organic Aerosol from isoprene above a maritime tropical forest, *Atmos. Chem. Phys.*, 11, 1039-1050, 2011, 10.5194/acp-11-1039-2011.
- Röhrh, A. and Lammel, G.: Determination of malic acid and other C4 dicarboxylic acids in atmospheric aerosol samples, *Chemosphere*, 46, 1195-1199, 2002, [https://doi.org/10.1016/S0045-6535\(01\)00243-0](https://doi.org/10.1016/S0045-6535(01)00243-0).
- Schneider, J., Weimer, S., Drewnick, F., Borrmann, S., Helas, G., Gwaze, P., Schmid, O., Andreae, M. O., and Kirchner, U.: Mass spectrometric analysis and aerodynamic properties of various types of combustion-related aerosol particles, *Int. J. Mass Spectrom.*, 258, 37-49, 2006, 10.1016/j.ijms.2006.07.008.
- Schneider, J., Freutel, F., Zorn, S., Chen, Q., Farmer, D., Jimenez, J., Martin, S., Artaxo, P., Wiedensohler, A., and Borrmann, S.: Mass-spectrometric identification of primary biological particle markers and application to pristine submicron aerosol measurements in Amazonia, *Atmos Chem Phys*, 11, 11415-11429, 2011, [doi.org/10.5194/acp-11-11415-2011](https://doi.org/10.5194/acp-11-11415-2011).
- Setyan, A., Zhang, Q., Merkel, M., Knighton, W. B., Sun, Y., Song, C., Shilling, J. E., Onasch, T. B., Herndon, S. C., Worsnop, D. R., Fast, J. D., Zaveri, R. A., Berg, L. K., Wiedensohler, A., Flowers, B. A., Dubey, M. K., and Subramanian, R.: Characterization of submicron particles influenced by mixed biogenic and anthropogenic emissions using high-resolution aerosol mass spectrometry: results from CARES, *Atmos. Chem. Phys.*, 12, 8131-8156, 2012, 10.5194/acp-12-8131-2012.
- Shilling, J. E., Zaveri, R. A., Fast, J. D., Kleinman, L., Alexander, M. L., Canagaratna, M. R., Fortner, E., Hubbe, J. M., Jayne, J. T., Sedlacek, A., Setyan, A., Springston, S., Worsnop, D. R., and Zhang, Q.: Enhanced SOA formation from mixed anthropogenic and biogenic emissions during the CARES campaign, *Atmos. Chem. Phys.*, 13, 2091-2113, 2013, 10.5194/acp-13-2091-2013.
- Shilling, J. E., Fortner, E., Pekour, M. S., Artaxo, P., Hubbe, J. M., Longo, K. M., Machado, L. A. T., Martin, S. T., Mei, F., Springston, S. R., Tomlinson, J., and Wang, J.: Particle-phase chemical composition measurements onboard the G-1 research aircraft during the GoAmazon2014/5 campaign in preparation.



- Shrivastava, M., Cappa, C. D., Fan, J., Goldstein, A. H., Guenther, A. B., Jimenez, J. L., Kuang, C., Laskin, A., Martin, S. T., Ng, N. L., Petaja, T., Pierce, J. R., Rasch, P. J., Roldin, P., Seinfeld, J. H., Shilling, J., Smith, J. N., Thornton, J. A., Volkamer, R., Wang, J., Worsnop, D. R., Zaveri, R. A., Zelenyuk, A., and Zhang, Q.: Recent advances in understanding secondary organic aerosol: Implications for global climate forcing, *Rev. Geophys.*, 55, 509-559, 2017, [10.1002/2016RG000540](https://doi.org/10.1002/2016RG000540).
- Spracklen, D. V., Jimenez, J. L., Carslaw, K. S., Worsnop, D. R., Evans, M. J., Mann, G. W., Zhang, Q., Canagaratna, M. R., Allan, J., Coe, H., McFiggans, G., Rap, A., and Forster, P.: Aerosol mass spectrometer constraint on the global secondary organic aerosol budget, *Atmos. Chem. Phys.*, 11, 12109-12136, 2011, [10.5194/acp-11-12109-2011](https://doi.org/10.5194/acp-11-12109-2011).
- Subramanian, R., Roden, C. A., Boparai, P., and Bond, T. C.: Yellow beads and missing particles: trouble ahead for filter-based absorption measurements, *Aerosol Sci Technol*, 41, 630-637, 2007, [10.1080/02786820701344589](https://doi.org/10.1080/02786820701344589).
- Sueper, D. and collaborators: ToF-AMS Data Analysis Software Webpage, [http://cires1.colorado.edu/jimenez-group/wiki/index.php/ToF-AMS\\_Analysis\\_Software](http://cires1.colorado.edu/jimenez-group/wiki/index.php/ToF-AMS_Analysis_Software), last access: August 2017.
- Surratt, J. D., Chan, A. W., Eddingsaas, N. C., Chan, M., Loza, C. L., Kwan, A. J., Hersey, S. P., Flagan, R. C., Wennberg, P. O., and Seinfeld, J. H.: Reactive intermediates revealed in secondary organic aerosol formation from isoprene, *Proc. Natl. Acad. Sci. USA*, 107, 6640-6645, 2010, [10.1073/pnas.091114107](https://doi.org/10.1073/pnas.091114107).
- Thalman, R., de Sá, S. S., Palm, B. B., Barbosa, H. M. J., Pöhlker, M. L., Alexander, M. L., Brito, J., Carbone, S., Castillo, P., Day, D. A., Kuang, C., Manzi, A., Ng, N. L., Sedlacek Iii, A. J., Souza, R., Springston, S., Watson, T., Pöhlker, C., Pöschl, U., Andreae, M. O., Artaxo, P., Jimenez, J. L., Martin, S. T., and Wang, J.: CCN activity and organic hygroscopicity of aerosols downwind of an urban region in central Amazonia: seasonal and diel variations and impact of anthropogenic emissions, *Atmos. Chem. Phys.*, 17, 11779-11801, 2017, [10.5194/acp-17-11779-2017](https://doi.org/10.5194/acp-17-11779-2017).
- Tsigaridis, K., Krol, M., Dentener, F. J., Balkanski, Y., Lathière, J., Metzger, S., Hauglustaine, D. A., and Kanakidou, M.: Change in global aerosol composition since preindustrial times, *Atmos. Chem. Phys.*, 6, 5143-5162, 2006, [10.5194/acp-6-5143-2006](https://doi.org/10.5194/acp-6-5143-2006).
- Ulbrich, I., Handschy, A., Lechner, M. J., and Jimenez, J.: AMS Spectral Database, 2009a, <http://cires.colorado.edu/jimenez-group/AMSsd/>, last access: August 2017.
- Ulbrich, I., Canagaratna, M., Zhang, Q., Worsnop, D., and Jimenez, J.: Interpretation of organic components from positive matrix factorization of aerosol mass spectrometric data, *Atmos. Chem. Phys.*, 9, 2891-2918, 2009b, [10.5194/acp-9-2891-2009](https://doi.org/10.5194/acp-9-2891-2009).
- Ulbrich, I., Handschy, A., Lechner, M. J., and Jimenez, J.: High-Resolution AMS Spectral Database, 2009c, <http://cires.colorado.edu/jimenez-group/HRAMSsd/>, last access: August 2017.
- van Pinxteren, D., Neusüß, C., and Herrmann, H.: On the abundance and source contributions of dicarboxylic acids in size-resolved aerosol particles at continental sites in central Europe, *Atmos. Chem. Phys.*, 14, 3913-3928, 2014.
- Weber, R. J., Sullivan, A. P., Peltier, R. E., Russell, A., Yan, B., Zheng, M., de Gouw, J., Warneke, C., Brock, C., Holloway, J. S., Atlas, E. L., and Edgerton, E.: A study of secondary organic aerosol formation in the anthropogenic-influenced southeastern United States, *J. Geophys. Res. Atmos.*, 112, D13302, 2007, [10.1029/2007JD008408](https://doi.org/10.1029/2007JD008408).



- Worton, D. R., Surratt, J. D., LaFranchi, B. W., Chan, A. W. H., Zhao, Y., Weber, R. J., Park, J.-H., Gilman, J. B., de Gouw, J., Park, C., Schade, G., Beaver, M., Clair, J. M. S., Crounse, J., Wennberg, P., Wolfe, G. M., Harrold, S., Thornton, J. A., Farmer, D. K., Docherty, K. S., Cubison, M. J., Jimenez, J.-L., Frossard, A. A., Russell, L. M., Kristensen, K., Glasius, M., Mao, J., Ren, X., Brune, W., Browne, E. C., Pusede, S. E., Cohen, R. C., Seinfeld, J. H., and Goldstein, A. H.: Observational insights into aerosol formation from isoprene, *Environ. Sci. Technol.*, 47, 11403-11413, 2013, [10.1021/es4011064](https://doi.org/10.1021/es4011064).
- Xu, L., Guo, H., Boyd, C. M., Klein, M., Bougiatioti, A., Cerully, K. M., Hite, J. R., Isaacman-VanWertz, G., Kreisberg, N. M., Knote, C., Olson, K., Koss, A., Goldstein, A. H., Hering, S. V., de Gouw, J., Baumann, K., Lee, S.-H., Nenes, A., Weber, R. J., and Ng, N. L.: Effects of anthropogenic emissions on aerosol formation from isoprene and monoterpenes in the southeastern United States, *Proc. Natl. Acad. Sci. USA*, 112, 37-42, 2015a, [10.1073/pnas.1417609112](https://doi.org/10.1073/pnas.1417609112).
- Xu, L., Suresh, S., Guo, H., Weber, R. J., and Ng, N. L.: Aerosol characterization over the southeastern United States using high-resolution aerosol mass spectrometry: spatial and seasonal variation of aerosol composition and sources with a focus on organic nitrates, *Atmos. Chem. Phys.*, 15, 7307-7336, 2015b, [10.5194/acp-15-7307-2015](https://doi.org/10.5194/acp-15-7307-2015).
- Yáñez-Serrano, A. M., Nölscher, A. C., Williams, J., Wolff, S., Alves, E., Martins, G. A., Bourtsoukidis, E., Brito, J., Jardine, K., Artaxo, P., and Kesselmeier, J.: Diel and seasonal changes of biogenic volatile organic compounds within and above an Amazonian rainforest, *Atmos. Chem. Phys.*, 15, 3359-3378, 2015, [10.5194/acp-15-3359-2015](https://doi.org/10.5194/acp-15-3359-2015).
- Zhang, H., Yee, L. D., and Goldstein, A. H.: Monoterpenes are the largest source of summertime organic aerosol in the southeastern United States, in press.
- Zhang, Q., Alfarra, M. R., Worsnop, D. R., Allan, J. D., Coe, H., Canagaratna, M. R., and Jimenez, J. L.: Deconvolution and quantification of hydrocarbon-like and oxygenated organic aerosols based on aerosol mass spectrometry, *Environ. Sci. Technol.*, 39, 4938-4952, 2005, [10.1021/es048568l](https://doi.org/10.1021/es048568l).
- Zhang, Q., Jimenez, J. L., Canagaratna, M. R., Ulbrich, I. M., Ng, N. L., Worsnop, D. R., and Sun, Y.: Understanding atmospheric organic aerosols via factor analysis of aerosol mass spectrometry: a review, *Anal. Bioanal. Chem.*, 401, 3045-3067, 2011, [10.1007/s00216-011-5355-y](https://doi.org/10.1007/s00216-011-5355-y).



## List of Figures

**Figure 1.** (a) Mass concentrations of PM<sub>1</sub> species at T3 during the wet season of 2014 (IOP1).

Non-refractory (NR) PM<sub>1</sub> species of organic, sulfate, ammonium, nitrate, and chloride were measured by the AMS. Mass concentrations of black carbon were obtained by scaling aethalometer measurements by a factor of 2 based on the range of 1 to 3 for the comparison of SP2 to aethalometer measurements. The temporal trend of the two instruments agreed well. (b) Comparison of the summed mass concentrations of non-refractory PM<sub>1</sub> species (top) and the mass fractions of these species (bottom) at T3 and three other regional sites. T0a-2015 refers to measurements in the wet season of 2015 at the ATTO location (Carbone et al., in preparation). T0t-2008 refers to the AMAZE-08 experiment, which took place in the wet season of 2008 at the TT34 location (Chen et al., 2015). T2-2014 refers to measurements made during IOP1 at a site 8 km downwind of Manaus, just across the Black River (“Rio Negro) (Brito et al., in preparation). Measurements at T0a in 2015 and at T2 in 2014 were made by an ACSM, and measurements at T0t in 2008 and at T3 in 2014 were made by an AMS. Concentrations were adjusted to standard temperature (273.15 K) and pressure (10<sup>5</sup> Pa). Bars represent means and whiskers represent the standard deviation of measurements.

**Figure 2.** Diel patterns of the mass concentrations of organic (top, green) and sulfate (bottom, red) species during the wet season at four different sites (cf. Fig. 1 and Fig. **Error! Reference source not found.**). Mass concentrations were corrected to standard temperature and pressure (273.15 K and 10<sup>5</sup> Pa). Local time is (UTC - 4 h). Lines represent means, solid markers show medians, and boxes span interquartile ranges.



The ordinate scale for the T2 panel differs from the other three panels. Concentrations were adjusted to standard temperature (273.15 K) and pressure ( $10^5$  Pa).

**Figure 3.** Scatter plot of the AMS signal fraction at  $m/z$  44 ( $f_{44}$ ) against that at  $m/z$  43 ( $f_{43}$ ). Gray and blue circles correspond, respectively, to measurements at T3 and T2 during IOP1, in the wet season of 2014. Solid squares represent median values, and whiskers represent 10 and 90 percentiles. Dashed lines delineate the region where worldwide measurements of ambient organic  $PM_{10}$  commonly lie (Ng et al., 2011a).

**Figure 4.** Results of the PMF analysis on the time series of AMS organic mass spectra collected at T3. (a) Mass spectral profile of each factor represented at unit mass resolution. The inset shows the mean fractional loading of each factor. (b) Diel trends for the loadings of each PMF factor. Local time is (UTC - 4 h). Lines represent means, solid markers show medians, and boxes span interquartile ranges. (c) Time series of the factor loadings (left axis) and other related measurements at T3 (right axis). Methyl-butyl-tricarboxylic acid is abbreviated as MBTCA.

**Figure 5.** Column plot of Pearson  $R$  correlations between the loading of each PMF factor and values of selected measurements at T3. Abbreviations include tricarballic acid (TCA), methyl-butyl-tricarboxylic acid (MBTCA), methyl vinyl ketone (MVK), methacrolein (MACR), and isoprene hydroxyhydroperoxides (ISOPOOH). SV-TAG measurements refer to particle-phase concentrations. Isomers could not be distinguished by PTR-ToF-MS measurements;  $C_8$  and  $C_9$  aromatics include the xylene and trimethylbenzene isomers, respectively.

**Figure 6.** Results of the cluster analysis by Fuzzy c-means (FCM) for afternoon periods (12:00 to 16:00 h) are presented by several case studies. (a) Degree of membership in each of



the four clusters. The sum of degrees of membership across all clusters is unity. Background conditions are abbreviated as “Bkgd”, and polluted conditions are abbreviated as “Pol”. (b) Pollution indicators: concentrations of  $\text{NO}_y$ ,  $\text{O}_3$ , black carbon (BC), and particle number count are plotted. (c)  $\text{PM}_{10}$  mass concentrations for organic, sulfate, nitrate, and ammonium species. (d) Fractional contribution of each factor to total organic  $\text{PM}_{10}$ .

**Figure 7.** Air mass backtrajectories associated with the four clusters of the FCM analysis for the case studies of Figure 6. Trajectories were calculated using HYSPLIT 4 in steps of 12 min for ten hours (Draxler and Hess, 1998). Image data: Google earth.

**Figure 8.** Characteristic PM composition of the FCM clusters as represented by coordinates of cluster centroids. (a) Mass concentrations of AMS species characteristic of each cluster. (b) PMF factor loadings characteristic of each cluster. Calculations are presented in more detail in the Supplementary Material (Section S3). Values plotted are shown in Table 2.

**Figure 9.** Schematic representation of (a) atmospheric processes, illustrated in a simplified manner, associated with the production of organic  $\text{PM}_{10}$  and (b) observables of these processes as captured by the datasets and analytical approach employed in this study. In panel (a), the left side depicts the emissions of biogenic volatile organic compounds (VOCs), their atmospheric oxidation, and the production of biogenic secondary organic  $\text{PM}_{10}$ . The right side depicts anthropogenic emissions of gas species and particulate matter that can alter natural atmospheric concentrations and processes. There are primary organic  $\text{PM}_{10}$  emissions from traffic, cooking, and industrial



activities. Anthropogenic VOCs can be precursors for the production of secondary organic PM<sub>1</sub> and can affect the production of ozone and hydroxyl radical. NO<sub>x</sub> emissions directly and indirectly alter the natural pathways of PM<sub>1</sub> production in the atmosphere. NO<sub>x</sub> and SO<sub>x</sub> can also directly contribute to the formation of secondary inorganic PM<sub>1</sub> (not shown), which can in turn play a role in changing pathways of secondary organic PM<sub>1</sub> production. In panel (b), different PMF factors represent distinct sources and/or processes. The IEPOX-SOA factor is at the intersection of the two, as it represents both a source (i.e., isoprene emissions from the forest) and a process (i.e., photo-oxidation under HO<sub>2</sub> dominant conditions, influenced by sulfate concentrations). The dashed black line represents the natural and anthropogenic oxidative processes that transform the chemical signature of the HOA, ADOA, BBOA, IEPOX-SOA, and LO-OOA factors after sufficient atmospheric residence time into the MO-OOA factor. The clusters represent different conditions at the receptor site (i.e., T3) and therefore incorporate the meteorological and geographical histories of the air masses that reach the site and affect the observed concentrations. The different PMF factors are associated to the different clusters (solid lines) to various extents (not detailed here for simplification purposes; cf. Figure 8).



**Table 1.** Characteristics of the PMF factors derived from the AMS datasets. Listed are signal fractions  $f_{\text{CO}_2^+}$  at nominal  $m/z$  44 and oxygen-to-carbon (O:C) and hydrogen-to-carbon (H:C) ratios. Values and associated uncertainties were calculated by running PMF in “bootstrap mode” (Ulbrich et al., 2009b). Elemental ratios were calibrated by the “improved-ambient” method, which has an estimated uncertainty of 12% for O:C and 4% for H:C (Canagaratna et al., 2015).

PMF factor	$f_{\text{CO}_2^+}$	O:C	H:C
MO-OOA	$0.25 \pm 0.01$	$1.09 \pm 0.17$	$1.27 \pm 0.12$
LO-OOA	$0.14 \pm 0.02$	$0.72 \pm 0.10$	$1.49 \pm 0.07$
IEPOX-SOA	$0.17 \pm 0.01$	$0.93 \pm 0.10$	$1.39 \pm 0.07$
ADOA	$0.11 \pm 0.01$	$0.40 \pm 0.05$	$1.63 \pm 0.02$
BBOA	$0.123 \pm 0.004$	$0.61 \pm 0.08$	$1.57 \pm 0.04$
HOA	$0.048 \pm 0.006$	$0.18 \pm 0.02$	$1.94 \pm 0.02$



**Table 2.** Coordinates of cluster centroids for input variables, AMS species concentrations, and PMF factor loadings. Table entries for AMS species and PMF factors are plotted in Figure 8. The AMS species concentrations (except for sulfate) and PMF factor loadings were not used as input variables in the FCM clustering analysis.

Species	Cluster Centroid			
	Bkgd-1	Bkgd-2	Pol-1	Pol-2
<b>Input variables</b>				
Particle number (cm <sup>-3</sup> )	714	1117	2636	6697
NO <sub>y</sub> (ppb)	0.64	0.95	1.2	2.2
O <sub>3</sub> (ppb)	14	17	26	36
Black carbon (μg m <sup>-3</sup> )	0.05	0.16	0.21	0.18
Sulfate (μg m <sup>-3</sup> )	0.15	0.36	0.44	0.57
<b>AMS species concentrations (μg m<sup>-3</sup>)</b>				
Organic	0.96	2.0	2.5	2.6
Ammonium	0.05	0.12	0.15	0.21
Nitrate	0.03	0.07	0.10	0.12
Chloride	0.007	0.011	0.009	0.007
<b>PMF factor loadings (μg m<sup>-3</sup>)</b>				
MO-OOA	0.29	0.83	1.13	1.13
LO-OOA	0.38	0.41	0.62	0.77
IEPOX-SOA	0.18	0.49	0.43	0.29
ADOA	0.044	0.086	0.19	0.32
BBOA	0.028	0.054	0.081	0.063
HOA	0.017	0.027	0.039	0.040

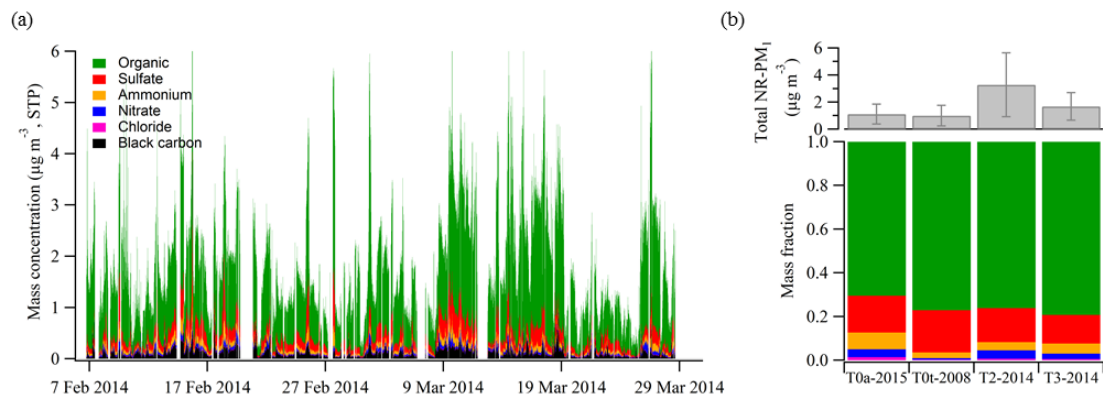


Figure 1

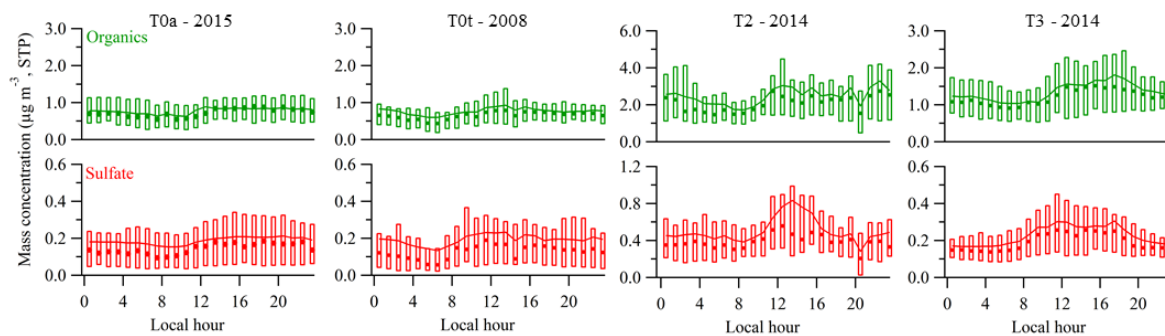


Figure 2

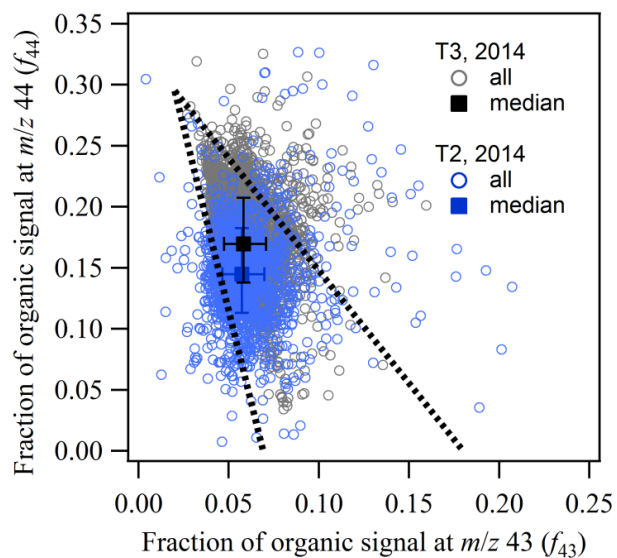


Figure 3

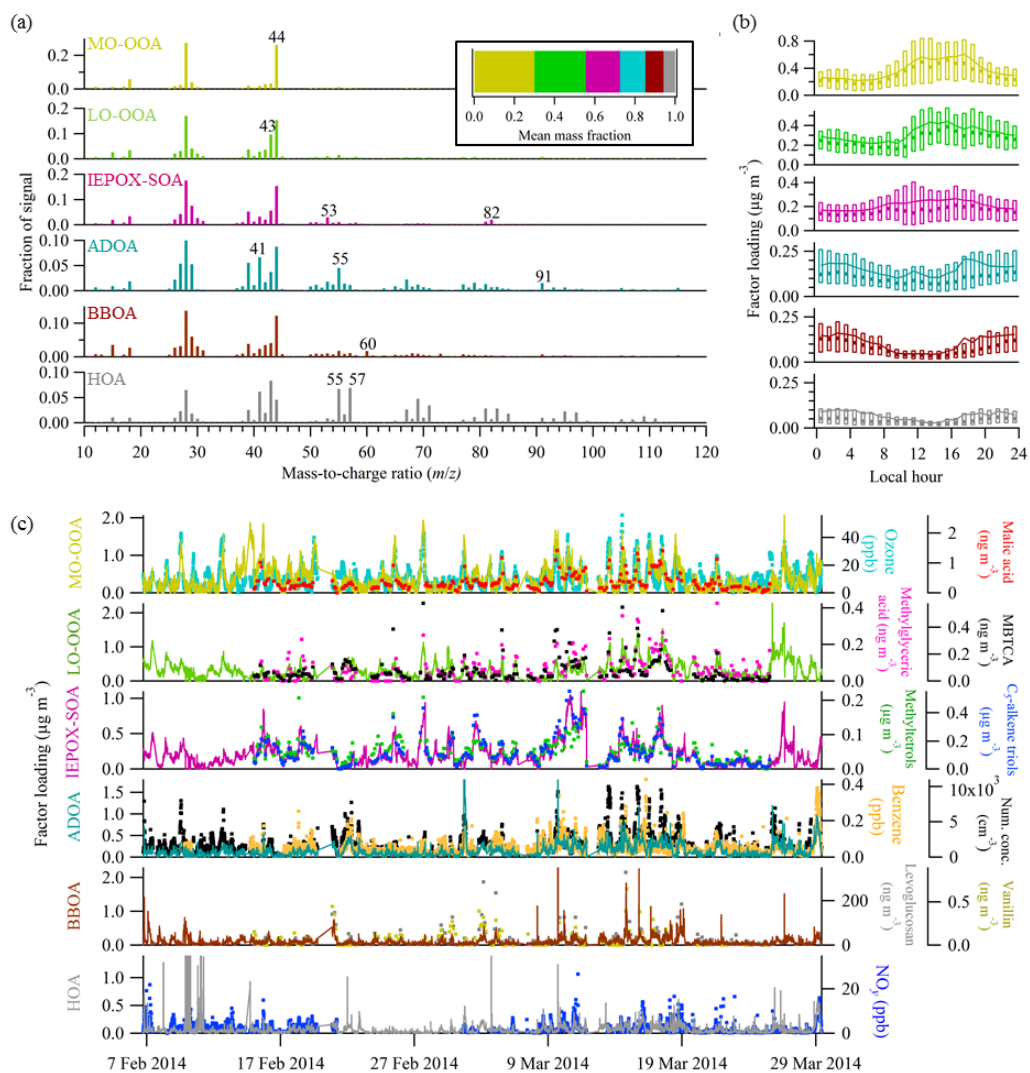


Figure 4

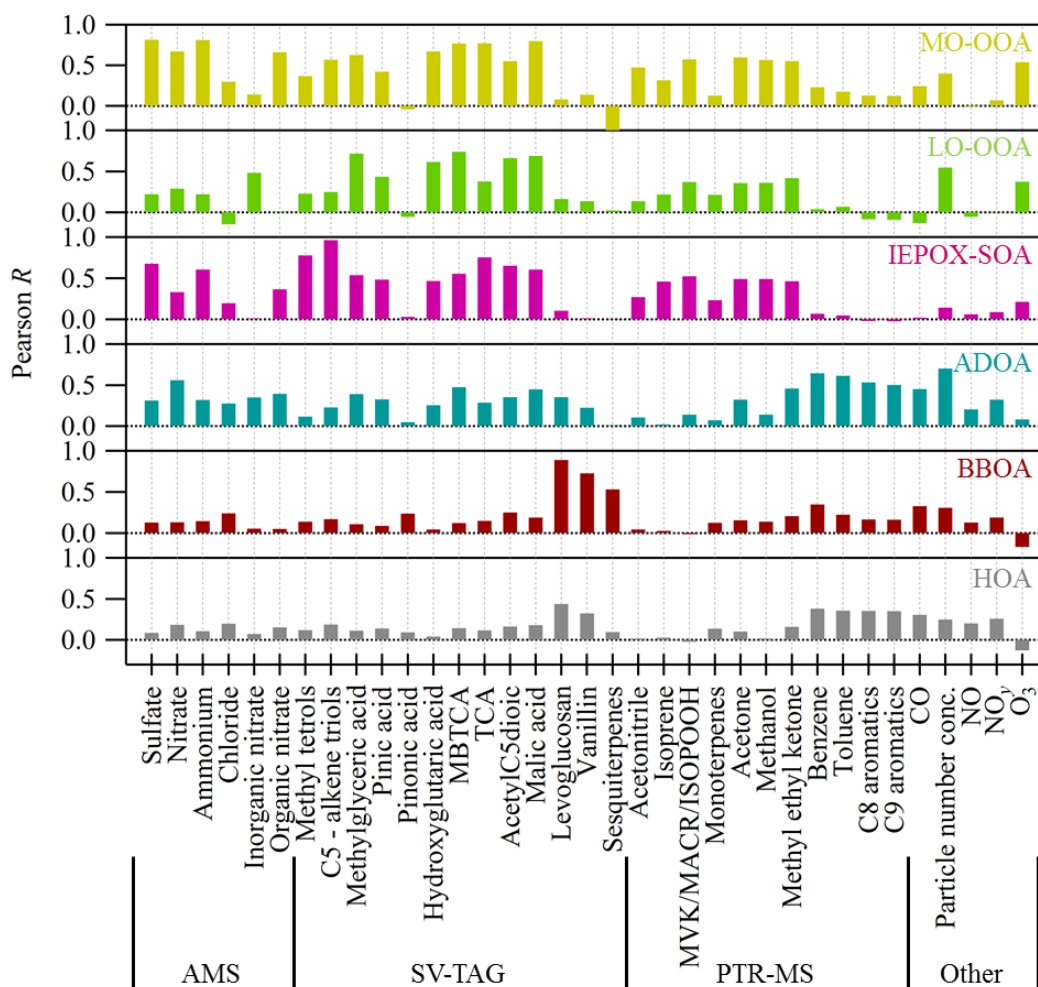


Figure 5

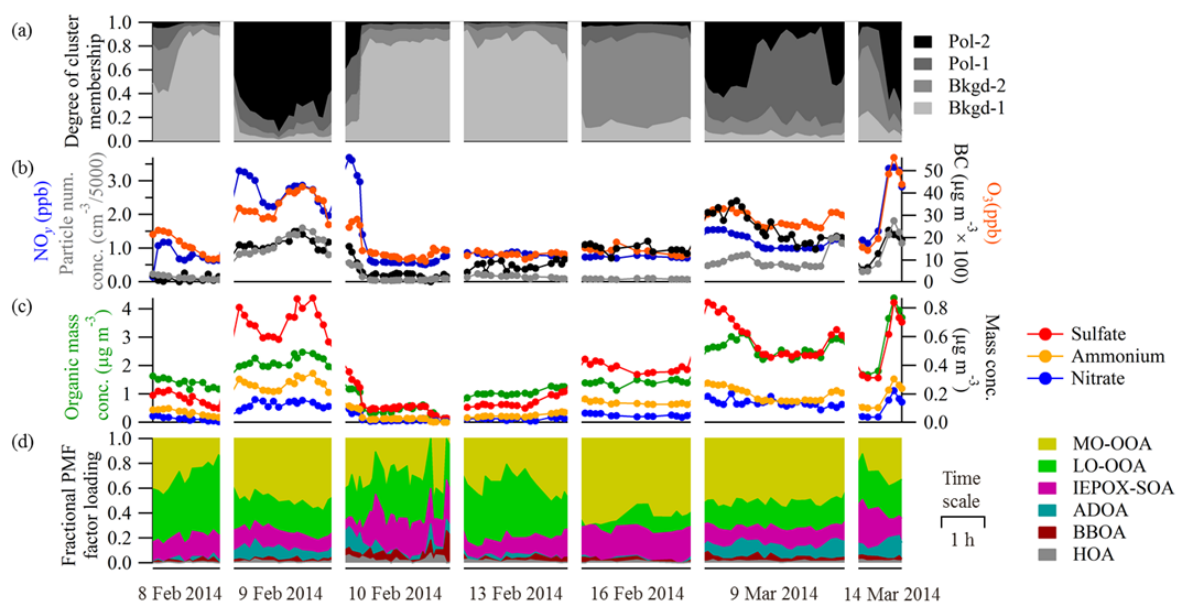


Figure 6

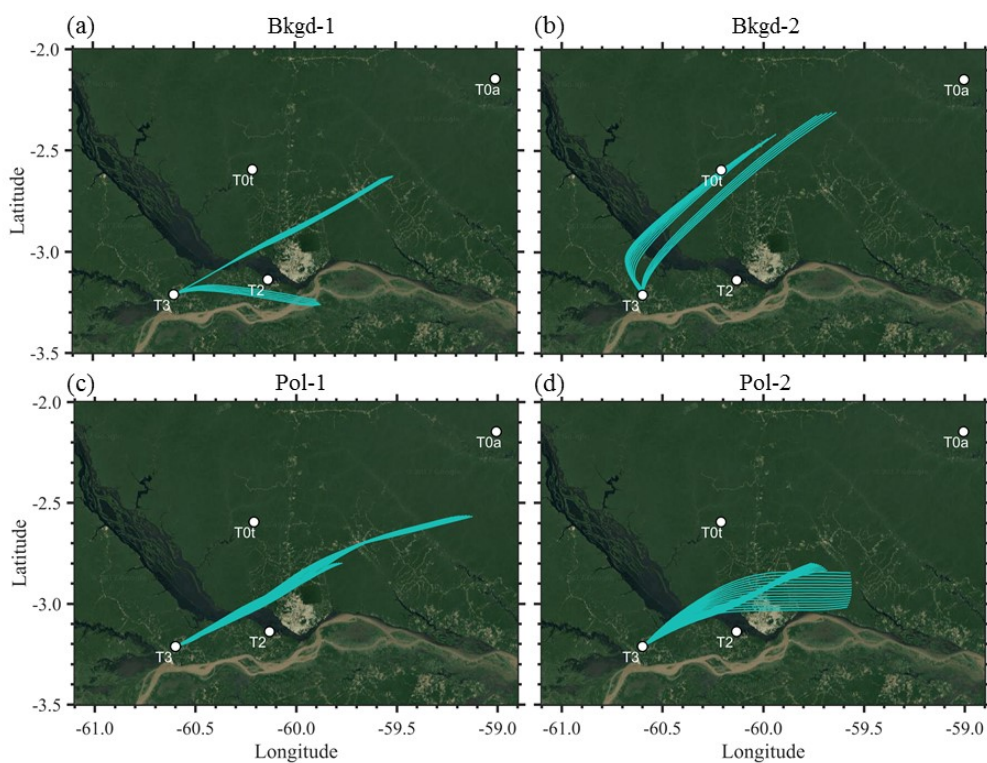


Figure 7

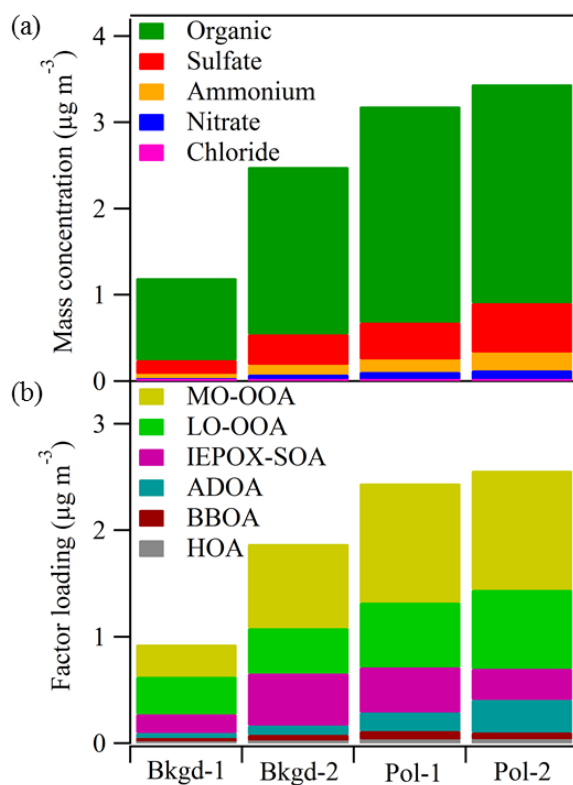


Figure 8

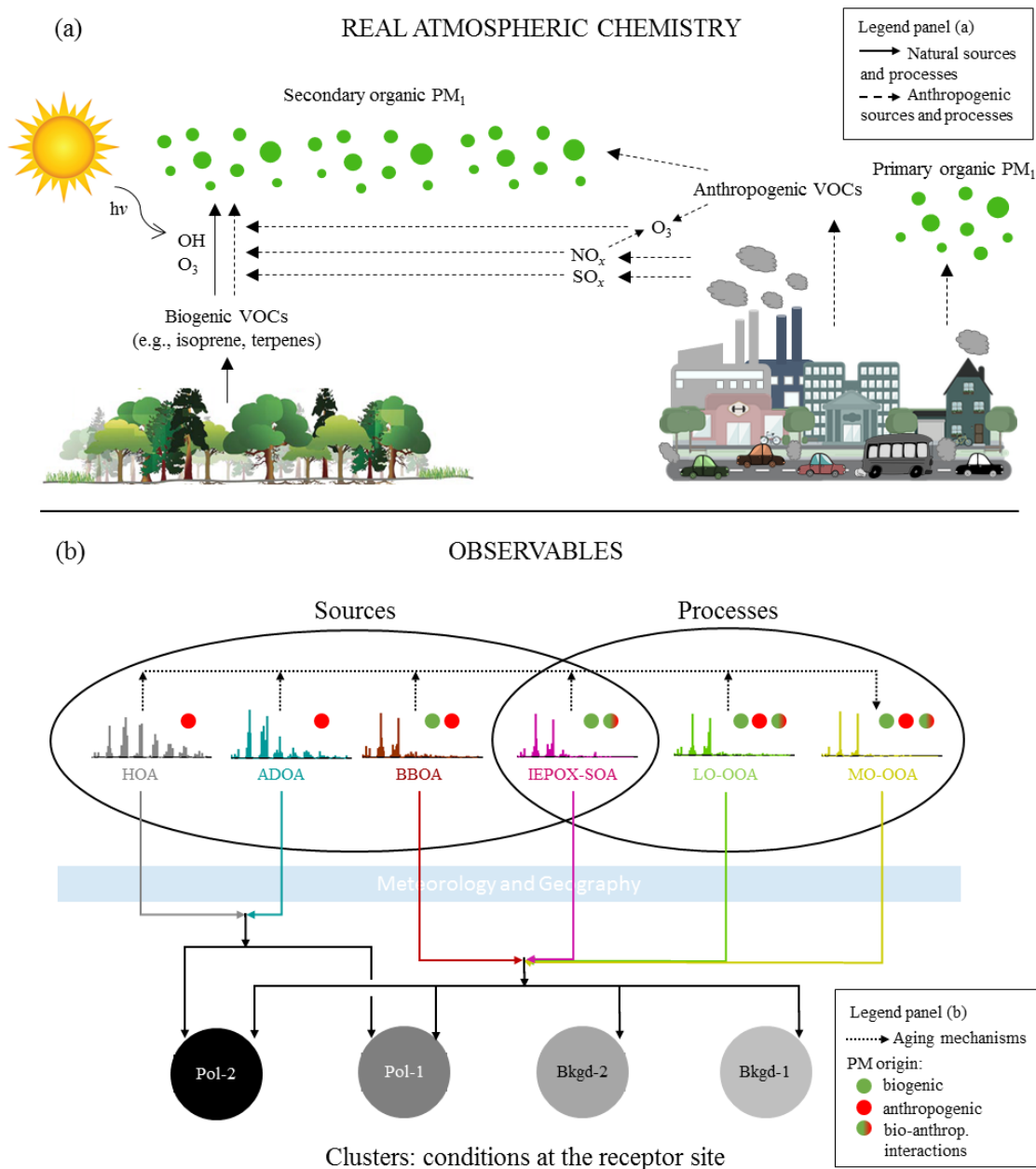


Figure 9